SAPIENZA
Università di Roma

PhD Programme in Life Sciences

XXXV Cycle

Novel insights into fungal degradation of lignin: role of a flavoenzyme in assisting laccase-mediated oxidations.

Candidate
Elena Gugole

Supervisor
Prof. Beatrice Vallone

Co-supervisor
Prof. Francesca Cutruzzolà

Tutor
Dr. Giuliano Sciara

Coordinator
Prof. Francesca Cutruzzolà

Table of contents

List of abbreviation

AA: auxiliary activity

AAD: aryl-alcohol dehydrogenase

AAO: aryl-alcohol oxidase

*Af*GDH: glucose dehydrogenase from *Aspergillus flavus*

*An*GOX: glucose oxidase from *Aspergillus niger*

AOX: alcohol oxidase

CAZy: carbohydrate active enzymes

CDH: cellobiose dehydrogenase

CHOX: choline oxidase

DAD: dehydrodisinapic acid dilactone

DCIP: 2,6-dicholorophenolindophenol

FAD: flavin adenine dinucleotide

GA: guaiacol

GDH: glucose dehydrogenase

GH: glucose hydrolase

GLC: D-glucose

GMC: glucose-methanol-choline

GOX: glucose oxidase

HBT: 1-hydroxybenzotriazole

LDAs: lignin-degrading auxiliary enzymes

LMB: laminaribiose

LMEs: lignin-modifying enzymes

LPMO: lytic polysaccharide monooxygenase 2

P2O: pyranose 2-oxidase

PDH: pyranose dehydrogenase

*Pc*ODH: oligosaccharide dehydrogenase from Pycnoporus cinnabarinus

*Pc*ODH-GA: guaiacol-bound *Pc*ODH

*Pc*ODH-GLC: glucose-bound *Pc*ODH

*Pc*ODH-LMB: laminaribiose-bound *Pc*ODH

*Pc*ODH-SA*t*: sinapic acid-bound *Pc*ODH (tetragonal space group)

*Pc*ODH-SA*o*: sinapic acid-bound *Pc*ODH (orthorombic space group)

*Pc*GDH r.m.s.d.: root-mean-square deviation

POX: pyranose oxidase

SA: sinapic acid

SBS: external sugar-binding site

TBDMS: tert-butyldimethylsilyl chloride

In all Figures, amino acid residues are indicated using a one-letter code.

Introduction

1.1 Biochemistry of plant cell wall degradation

Plant cell wall is a complex matrix that surrounds plants' cells[1]. It is involved in many functions such as providing shape and strength to the plant body and in plant growth, cell differentiation, intercellular communication and water movement. One of its main roles is to provide protection against possible pathogens attack[1,2].
Plant cell walls can be categorized as *primary* and *secondary:* the first surrounds growing cells, the second is characterized by a thicker structure and it is typical of conduction or support tissues[2]. The secondary plant cell wall is found in plants that require great mechanical strength and structural reinforcement[1], appears when the plant cell has stopped expanding and, in some cases, produces wood.
From a chemical point of view, the woody plant material is composed of hemicellulose, cellulose, and lignin (***Figure 1.1***).
Cellulose is a polymer of glucose, in which each monomer is connected by β-1,4 bonds; chains are held together in a crystalline structure by hydrogen bonds and van der Waals forces to form microfibrils[3]. Hemicellulose is a heterogeneous, branched polysaccharide primarily composed of β-1,4 linked polymers including xylan, glucoronxylan, xyloglucan, glucomannan, and arabinoxylan backbones, with heterogeneous side chains[4]. Lignin is a heterogeneous poly-phenolic polymer linked by C−O and C−C bonds[4].
Lignin and hemicellulose polymers form a complex matrix and function as adhesive for cellulose microfibrils. This molecular architecture is highly recalcitrant to both chemical and biological degradation, forming a strong, hydrophobic, insoluble barrier that protects the cellulose polymer against hydrolytic attack by most pathogenic and saprophytic organisms[5].
Such complex and intricate structures require an elaborate degradation system. Organisms belonging to different kingdoms of life have evolved enzymatic mechanisms to access and utilize cellulose as a

source of food and energy. To do so, they utilize enzymes that act synergistically to break down polysaccharides[4] and lignin[6]. Of all biomass-degrading organisms, fungi are responsible for the degradation of the majority of biomass in nature[4].
Attack on the polysaccharide backbone is carried out by the synergistic activity of glycoside hydrolase and lytic polysaccharide monooxygenase (LMPO)[4,7].

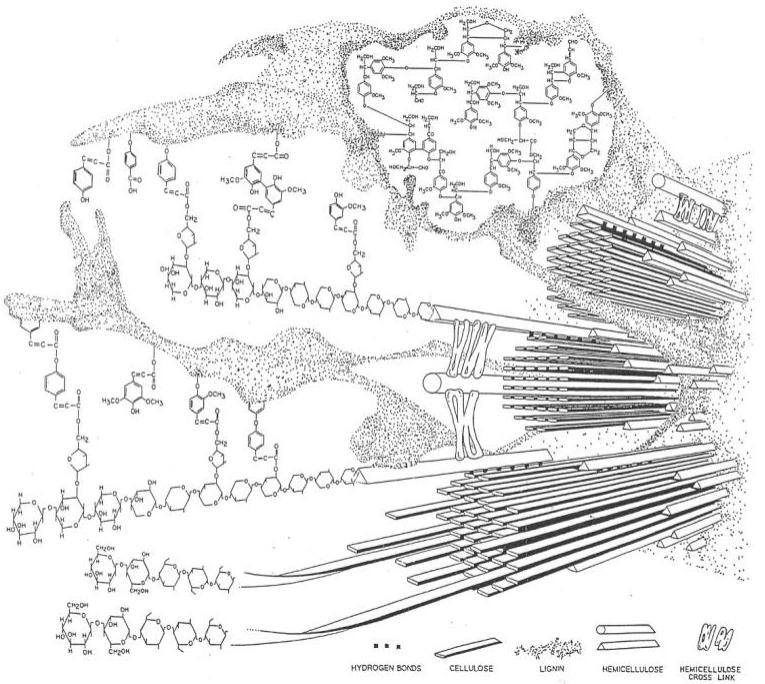

Figure 1.1 *Structure of lignocellulose: each component is pictured in its chemical form and interactions. Hemicellulose and lignin are adhesives that hold cellulose microfibrils of cellulose*[8].

The first one breaks glycosidic bonds by endo- and exo-hydrolytic activity on more accessible regions of cellulose, producing monomers of glucose.
They are supported by the LMPO enzymes that are able to create chain breaks in the crystalline regions of cellulose where the (GH) would not

be able to access[4] and can provide new chain ends as starting points for the hydrolases[7]. LPMOs hydroxylate the polysaccharide backbone via a single active-site copper ion[7].

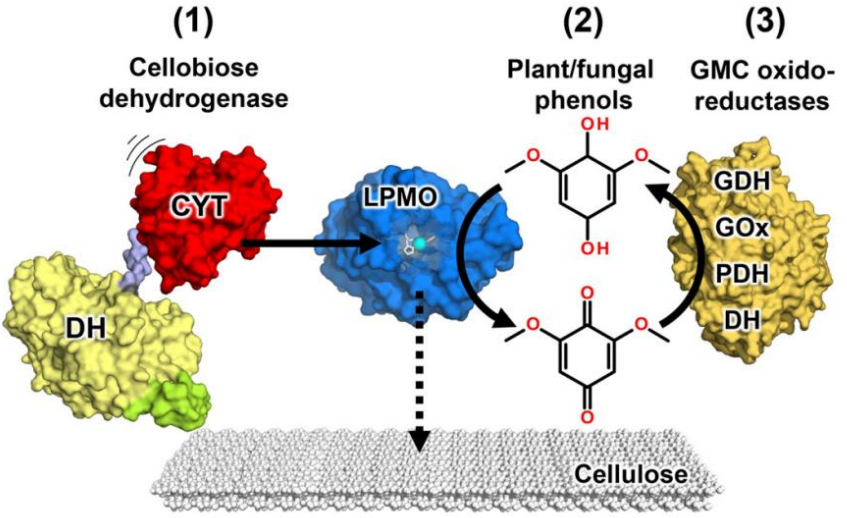

Figure 1.2 *Cellulose degradation performed by LPMO (cyan). The three electron transfer systems that support LPMO are depicted as follows: (1) CDH and its mobile cytochrome domain (red); (2) phenols derived from lignin degradation that directly reduce LPMO; (3) GMC oxidoreductases, such as glucose dehydrogenase (GDH), glucose oxidase (GOx), and pyranose dehydrogenase (PDH), as well as the DH domain of CDH, reduce phenols to quinones to fuel the activity of LMPO*[7].

To activate oxygen, LMPO enzymes must be reduced. At least three electron transferring systems reduce LPMOs during fungal lignocellulose attack (***Figure 1.2***). They can be directly reduced by the extracellular flavocytochrome CDH (System1), indirectly by members of the GMC oxidoreductases (System 3) that employ lignin-derived or fungal diphenols as redox mediators. These compounds (System 2) can efficiently reduce LPMO in the absence of regenerating enzymes but are irreversibly depleted by LPMO activity[4]. The importance of

LMPO in the biomass degradation process is also supported by the fact that genes encoding LPMO are found in 92% of fungal genomes.
Lignin degradation is carried out by two groups of enzymes: the Lignin Modifying Enzymes (LME) that catalyse the oxidative attack on lignin to decompose it in small parts, and the Lignin-Degrading Auxiliary enzymes (LDA) that support the first ones as reduction potential reserve to support the LDE[8].
Initially, enzymes that cleave complex carbohydrates were classified in the Carbohydrate Active enZymes (CAZy)[9], which includes glycoside hydrolases (GH), polysaccharide lyases (PL), carbohydrate esterases (CE), and glycosyltransferases (GT). Recently, the CAZy database has undergone rearrangements, and the families of lignin degradation enzymes are now grouped together with the LPMO families[10]. This resulted in a new CAZy class the "auxiliary activities" (AA)[11].
Although LDA and LME enzymes are not active on carbohydrates, the intimate association of lignin with the carbohydrates of plant cell walls makes the cooperation of ligninolytic and polysaccharide depolymerases inevitable.
Lignocellulose could contribute significantly to energy, material, and chemical production[4]. In particular, lignin is a potential source of biofuel and aromatic chemical compounds with applications in the pharmaceutical, alimentary, and cosmetic industries. However, it is undervalued and regarded as a low-value product in most biorefinery processes and in the paper pulp industry[12].

1.2 Lignin: structure, properties and its enzymatic degradation

Lignin is one of the three components of lignocellulosic biomass and after cellulose is the second most abundant biopolymer in nature. Indeed, lignin degradation is necessary for carbon recycling on earth[13]. From a chemical point of view, lignin is a complex heterogeneous phenolic polymer that provides support and protection to the woody plants' cell wall[8]. The appearance of lignin in the plant cell wall and its increasingly complex chemical structure are correlated with the evolution of higher plants (from ancient pteridophytes and gymnosperms to the most evolved grasses[14]): the water and nutrient transport required rigid tubular structures, while the strength and rigidity given by the interconnection of cellulose, hemicellulose, and lignin allowed trees to support their weight and face adverse weather[8].
The chemical structure of lignin is the result of the oxidative coupling of three phenolic monomers (monolignols), which are hydroxycinnamyl alcohols that differ mainly in the extent of methoxylation[6]: p-coumaryl, coniferyl, and synapyl alcohols (***Figure 1.3 A***). Lignification is the result of radical coupling of polymers or monomers oxidized by peroxidases, which leads to an arrangement of units linked by carbon–carbon and carbon–oxygen (ether) bonds[13]. The most common bonds are shown in ***Figure 1.3 B***.
Lignin composition is influenced by plant species and environmental factors, resulting in different molecular weights or linkage-motif percentages.
The heterogeneous structure of lignin makes its degradation complicated and accessible to only a restricted number of species, particularly fungi and some ligninolytic bacteria. The exact number of fungal species capable of degrading lignin is unknown; in 1980 Gilbertson[15] reported 1700 species of wood-degrading fungi in North America. This wood degrading fungi live as saprotrophic in forest ecosystems and are divided in three main groups (whites-root, brown-root, soft rot fungi) according to the morphology of the wood decomposed[8,16].

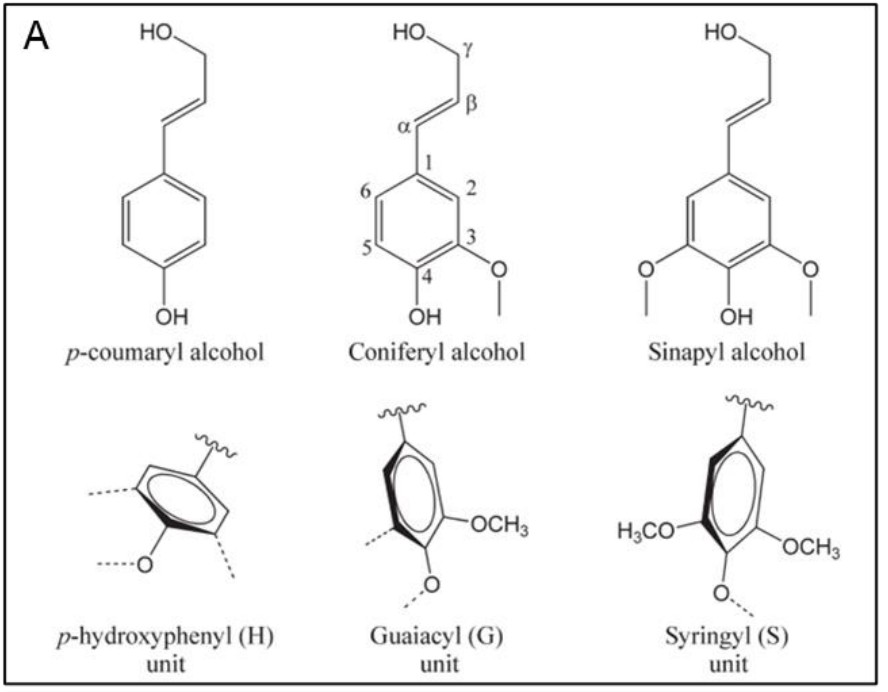
A
HO
OH
p-coumaryl alcohol
HO
γ
β
α
1
2
3
4
5
6
O
OH
Coniferyl alcohol
HO
O
O
OH
Sinapyl alcohol
O
p-hydroxyphenyl (H) unit
OCH3
O
Guaiacyl (G) unit
H3CO
OCH3
O
Syringyl (S) unit

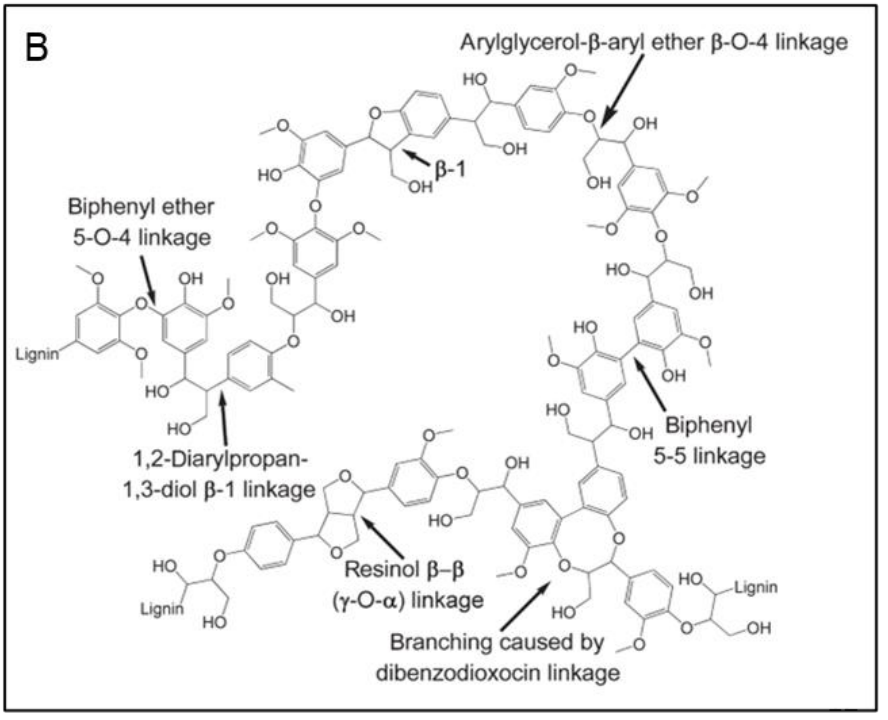
B
Arylglycerol-β-aryl ether β-O-4 linkage
β-1
Biphenyl ether
5-O-4 linkage
Lignin
1,2-Diarylpropan-
1,3-diol β-1 linkage
Biphenyl
5-5 linkage
Resinol β–β
(γ-O-α) linkage
Branching caused by
dibenzodioxocin linkage
Lignin
Lignin

*Figure 1.3 (**A**) Structures of monolignols (top) and corresponding units found in lignin (bottom) are indicated as p-hydrophenyl (H), guaiacyl (G), and syringyl (S) units. (**B**) Schematic representation of lignin*[13].

The breakdown of lignin by fungi is a fundamental function in the ecosystem because it prevents the accumulation of dead wood and allows the recycling of carbon; in fact, it exposes plant carbohydrates for microbial degradation[8,17].

White-root fungi are the primary degraders of lignin and are the only organisms capable of mineralizing it to CO_2 and H_2O. They owe their ability to degrade lignin to a cocktail of enzymes that carry out an oxidative attack that has come to be known as "enzymatic combustion"[18]. These enzymes are generally divided into two groups: lignin-modifying enzymes (LME) and lignin-degrading auxiliary (LDA) enzymes. LDA support LME enzymes during lignin degradation and are necessary to complete it.

LME are classified as lignin peroxidases (LiPs), manganese peroxidases (MnPs), versatile peroxidases (VPs), and (phenol-oxidases) laccases (***Figure 1.4 A***).

Lignin peroxidases (LiPs, AA2) contain an iron protoporphyrin IX (heme b) as the prosthetic group, like other peroxidases, and utilize H_2O_2 to catalyse the oxidation of their substrates[17] (***Figure 1.4 B)***.

LiPs are relatively nonspecific to their substrates; in fact, they can oxidize different phenolic aromatic compounds (guaiacol, vanillyl alcohol, and catechol) and a variety of non-phenolic lignin methoxyl-substituted lignin subunits[19]. This is possible because of the high redox potential of these enzymes, which is beyond the usual redox potential of plant peroxidases[20]. The substrate is oxidized to an aryl cation radical, which, in turn, generates different products resulting from ring cleavage and/or polymerization. These last reactions are non-enzymatic[17]. Mn-dependent peroxidases (MnPs, AA2) oxidize various phenolic compounds via one-electron extraction. This generates a phenoxy radical intermediate, which undergoes non-enzymatic reactions, leading to bond cleavages[17]. MnP is not able to catalyze the oxidation of non-phenolic compounds, but it can utilize Mn(III),

which can act as a low-molecular-weight mediator and oxidize molecules that require a higher redox potential[21].

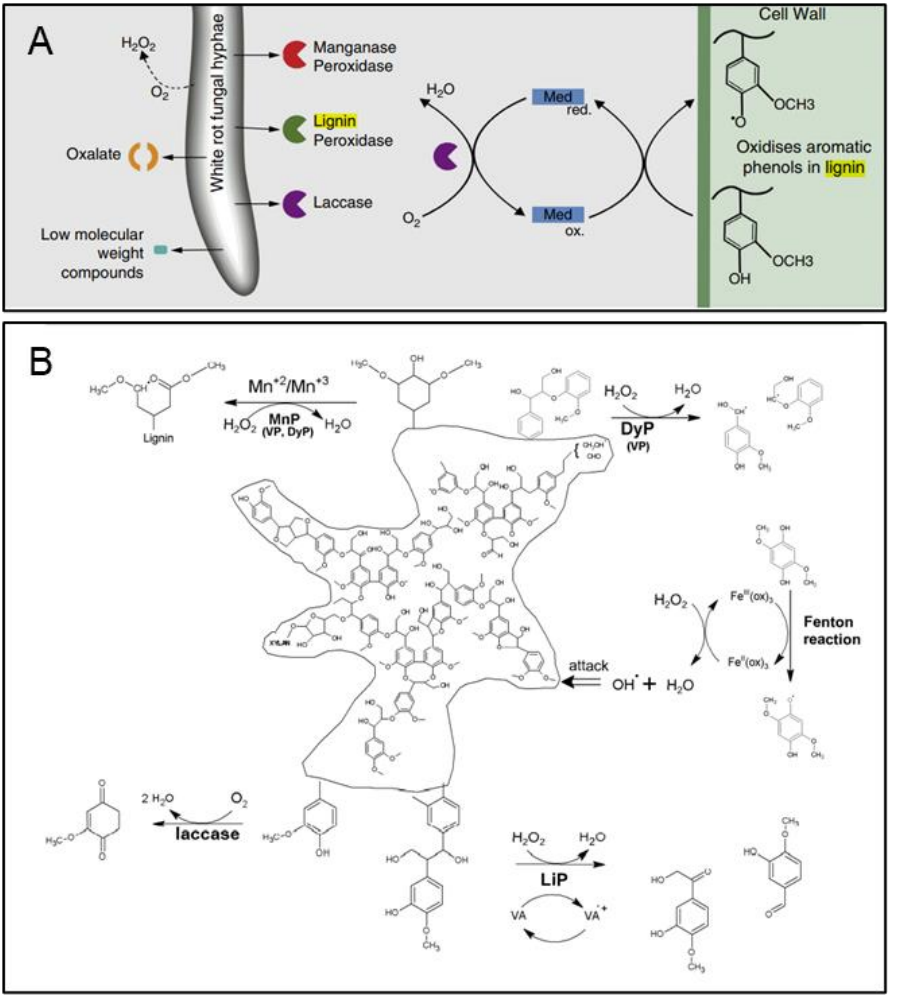

Figure 1.4 *(**A**) Lignin degradation by white-rot fungi. Enzymes such as peroxidase and laccase are secreted to perform a synergistic action in the degradation of lignin*[6]*. (**B**)Details of the reactions involving lignin-degrading enzymes. MnP: manganese peroxidase; VP: versatile peroxidase; LiP: lignin peroxidase; DyP: dye-decolorizing peroxidase; ox: oxalate; VA: veratryl alcohol. In parentheses, other enzymes capable to catalyze similar reaction are presented*[8]*.*

Versatile peroxidase (VPs, AA2) owes its name for its similarities with the other two peroxidases. In fact, it is capable of oxidizing the same substrates as LiP, but also nonphenolic compounds that require a high reduction potential[8]

It is important to note the role of low-molecular-weight mediators. These small molecules can act as mediators between lignin-degrading enzymes and lignin. They are necessary because enzymes are too large to penetrate the intricate lignin material, especially during the early stages of lignin degradation. They are usually ROS (hydroxyl radical, superoxide anion radical, hydrogen peroxide) produced by peroxidases and Fenton reactions, which can react directly with lignin and generate a cascade of bond breaks[8].

Among white-rot fungi, *Pycnoporus cinnabarinus* is a primary degrader of lignin. Sequencing of its genome provided an explanation for its outsdanding capacities: it possesses a wide range of enzymes that allow for efficient and complete degradation of lignin. The *genus Pycnoporus* belongs to the phylum Basidiomycota, class Agaricomycetes, order Polyporales, and family Polyporacae, and accounts for four species. Its name originates from the pigments cinnabarin and cinnabarinic acids, which give it a characteristic orange color[22].

1.3 Laccase enzymes

Laccases (AA1) have been found in almost all wood-rotting fungi and are ubiquitary enzymes[23]. They catalyze the oxidation of phenolic lignin derived molecules using oxygen as an electron acceptor.

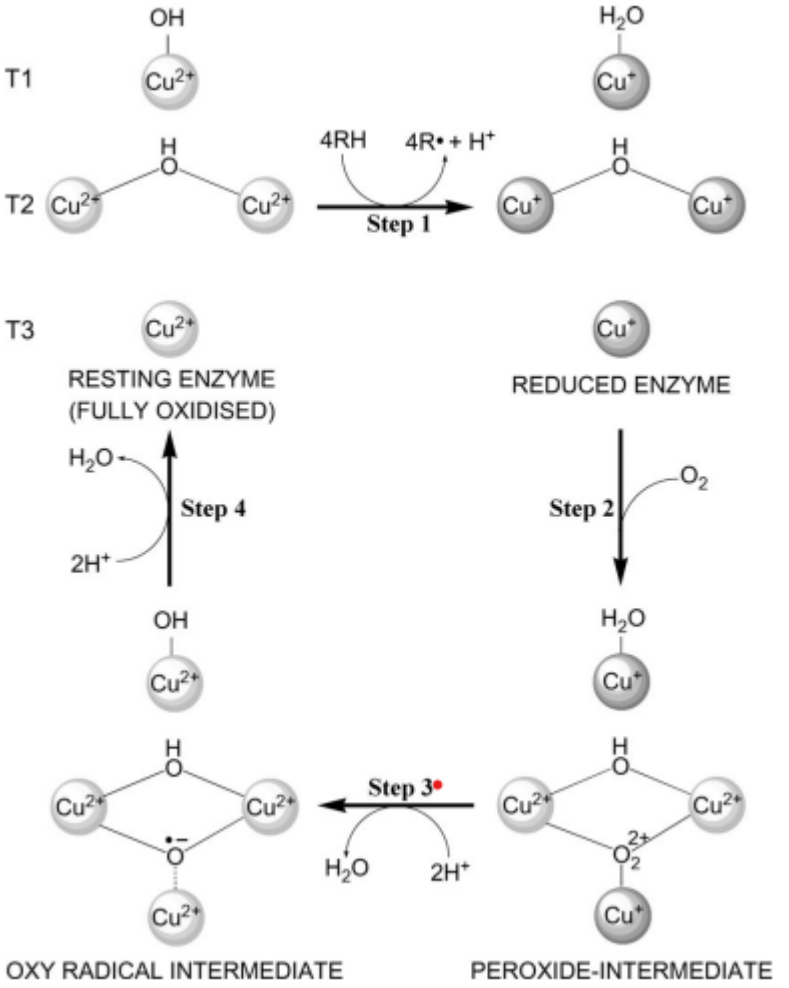

Figure 1.5 *Proposed mechanism catalytic cycle of laccase*[19,24,25].

Four Cu atoms execute the oxidation process and form the catalytic core of the enzyme. The four copper atoms are classified into three categories according to their UV-Vis and electronic paramagnetic characteristics: (*i*) type 1 (T1Cu) absorbs at 600 nm and gives a blue colour to the enzyme (when in the oxidized state); (ii) type 2 (T2Cu) is only detectable by EPR; (iii) type 3 (T3Cu) gives a weak absorption signal in the near-UV region. One T2 copper ion and two T3 copper ions are associate to form a trinuclear cluster (T2/T3) involved in the enzyme catalytic mechanism.

Figure 1.5 depicts a typical catalytic cycle of a laccase. First, the reducing substrate binds to T1 Cu and is oxidized; the electron that has been extracted is transferred to the trinuclear core. The enzyme is fully reduced after four-electron oxidations. Subsequently, oxygen binds to the T2/T3 core and is converted to a peroxide intermediate with two electron transfers from T3. Later two reductive electron cleavages of the O–O bond produce water. At the end 4 molecule of the substrate are oxidized to phenoxy radicals, and two molecules of water are produced[17]. This catalytic cycle can be summarized as a four-single-electron substrate oxidation reaction to reduce the enzyme and two consecutive two-electron steps to reduce O_2 to two water[17].

Laccase subtract one electron from the phenolic OH-group of phenolic compounds generating unstable phenoxy-radicals that undergo radical coupling leading to Ca oxidation, alkyl-aryl cleavage and Ca-Cb cleavage (***Figure 1.6 A***)[26,27].

Laccases do not have a sufficiently high reducing potential to oxidize nonphenolic compounds; however, the presence of mediators can enhance the oxidative capabilities of laccases. These compounds can be small molecular weight compounds (such as ROS) and extracellular natural aromatic compounds, such as p-hydroxycinnamic acids (p-coumaric, ferulic acid, and sinapic acid)[28], or synthetic compounds such as 1-hydroxybenzotriazole (HBT).

An example of possible product of laccase oxidation of a nonphenolic b-O-4 model compound in the presence of mediator HBT is reported in ***Figure 1.6 B***.

Numerous fungal laccases have been crystallized and their structures have been resolved. They share a common structural architecture

composed of three sequentially arranged cupredoxin-like domains[23], consisting of greek key β-barrel topology. The third domain usually contains T1 Cu, while T2 Cu and T3 Cu are coordinated with residues belonging to the first and third domains. The trinuclear centre is organized in a triangular shape and coordinated with four conserved His-X-His motifs[23].

The substrate-binding site is in a negatively charged cavity close to the T1 site. Substrate-binding cavities are usually wide, and they can accommodate a large variety of substrates and allow laccases to oxidize a variety of substrates that can be encountered during lignin degradation.

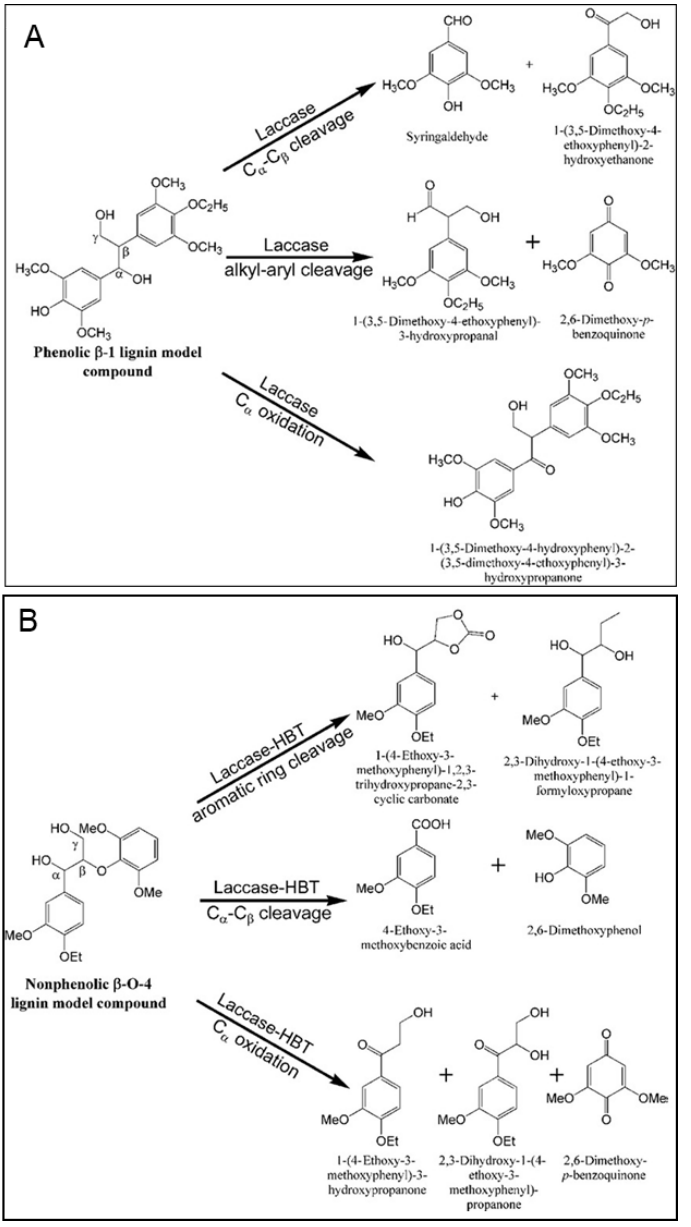

Figure 1.6 *(**A**) Three different possible products of laccase oxidation of phenolic b-1 lignin model compounds. (**B**) Three different products of HBT-mediated laccase oxidation*[13].

1.4 Multienzymes systems involved in the degradation of lignocellulose

Lignocellulose degradation is a complex process executed by numerous enzymes that act synergistically to perform enzymatic combustion (in the case of lignin) and hydrolytic actions (polysaccharides). These enzymes cooperate to achieve the degradation of lignocellulose (***Figure 1.7***). As previously mentioned, LDA enzymes carry on their functions in support of LME enzymes; in fact, they are not able to degrade lignin on their own, but they are necessary to complete the process[8]. They are thought to fulfil their support function by producing hydrogen peroxide from oxygen (necessary for the action of peroxidases[8,11]), reducing free radicals resulting from the activity of laccase (thus preventing repolymerization)[29,30], and quenching quinones that are then reused by LPMO machinery[31]. The LDA group includes glyoxal oxidase, which generates extracellular hydrogen peroxide and is classified in the family AA5[32–34], heme-thiolate peroxidases (chloro perosidases and aromatic peroxydases), and other members of the AA3 family[8].

The CAZy Auxiliary Activity family 3 (AA3) comprises members of the GMC (glucose-methanol-choline) oxidoreductases and depends on FAD as a cofactor. The AA3 family is divided into four subfamilies: cellobiose dehydrogenase (CDH, AA3_1), aryl alcohol oxidoreductase (AAO, AA3_2), glucose oxidase (GOX, AA3_2), glucose dehydrogenase (GDH, AA3_2), pyranose dehydrogenase (PDH, AA3_2), alcohol oxidase (AOX, AA3_3), and pyranose oxidase (POX, AA3_4).

Their actions also play a protective function, not only in deactivating reactive products generated by the lignin decomposition process but also in response to plant defense mechanisms. In fact, plants usually produce toxic quinones or radicals that induce repolymerization in response to fungal attack[8].

Recent secretome studies on the white rot fungus *Pycnoporus cinnabarinus* supported the role of AA3 enzymes in assisting lignin-degrading enzymes: the oxidative enzymes (AA2-LiP) were secreted with partner enzymes glyoxal oxidase (AA5_1) and GMC oxidoreductase (AA3_2). They were both detected on day 7 of

cultivation in lignocellulose medium[35]. The enzymes of this family not only support the enzymes that directly degrade lignin but also play a role in the earlier stages of hydrolysis of hemicellulose and cellulose. An example is CDH that behaves as an electron donor for LMPO and fuel its activity: transcriptome studies showed a similar transcription

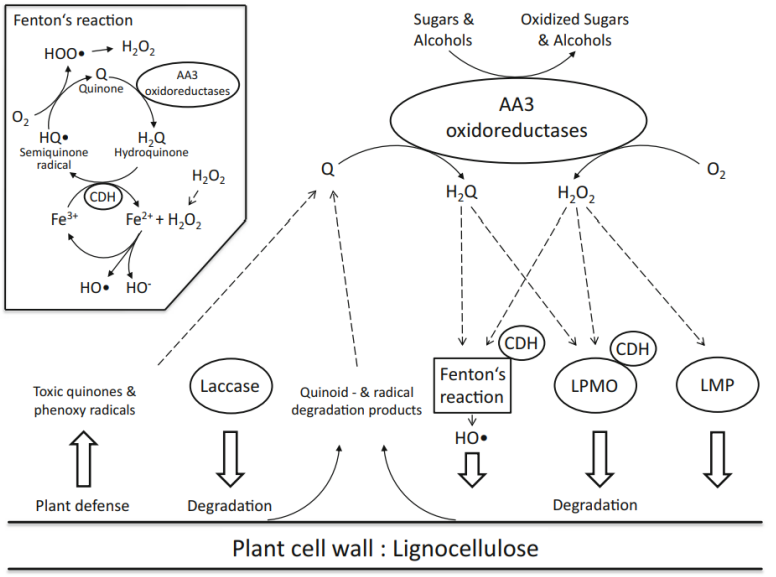

Figure 1.7 *AA3 enzymes activities during lignocellulose breakdown and their possible relevant interactions as multi-enzyme systems. The main products of AA3 actions are as follows: (i) H_2O_2 can fuel lignin-modifying peroxidases (LMP) and lytic polysaccharide monooxygenases (LPMO) and can be used in the Fenton reaction to produce radicals that can attack lignin; (ii) hydroquinones (H2Q), possibly produced by AA3 dehydrogenases, can be direct electron sources for LPMO and can participate in Fenton's reaction cycle. Quinones (Q) and radicals produced by lignin degradation or plant defenses can be reduced by AA3 dehydrogenase activity. Cellobiose dehydrogenase (CDH) directly reduces LPMO and is able to reduce Fe3+ ions in Fenton chemistry*[11].

pattern with AA9 LMPO enzymes (whose activity is described in paragraph 1.1). They are both upregulated and secreted during growth on cellulose[36].

All the AA3 enzymes belong to the GMC superfamily and share a common fold. They are typically composed of two major structural domains: a FAD-binding domain and a substrate-binding domain. The first one is highly conserved in all members and contains a conserved βαβ mononucleotide-binding motif, while the substrate-binding domain shows more sequence and structural variations, reflecting the different substrate specificities of the family.

Despite their wide range of possible substrates, they share an overall reaction mechanism that can be separated into two half-reactions: the first phase, in which the substrate is oxidized, reducing FAD to the reduced state (FADH2), and a second phase, in which FAD returns to the resting (oxidized) state by reducing the electron acceptor[11].

Structural, functional, and theoretical studies have shown that a highly conserved catalytic His/His or His/Asn pair in the active site is involved in the catalytic cycle[37]. The accepted hypothesis is that they act as a catalytic base for hydride abstraction during substrate oxidation[37–39].

In GMC oxidoreductase, the catalytic site is located at the base of a cavity that connects the isoalloxazine ring of the cofactor with the external environment. The geometry of the cavity varies among family members, accounting for different substrates and cofactor properties.

Regarding conformational changes induced by substrate binding, the family members (whose crystallographic structures have been resolved) showed greater variability. In the case of GDH and CDH, slight differences in the position of active site side chains were observed; in the case of AAO, no difference was observed, showing a pre-organized active site, and the only one that showed a closure mechanism was P2O.

Most of the GMC members possess a non-covalently bond FAD, except for CHOX[40], P2O[41] and PDH[42]. It is positioned in a narrow cavity and interacts with the protein environment mostly via hydrogen bonds, using several water molecules as bridges.

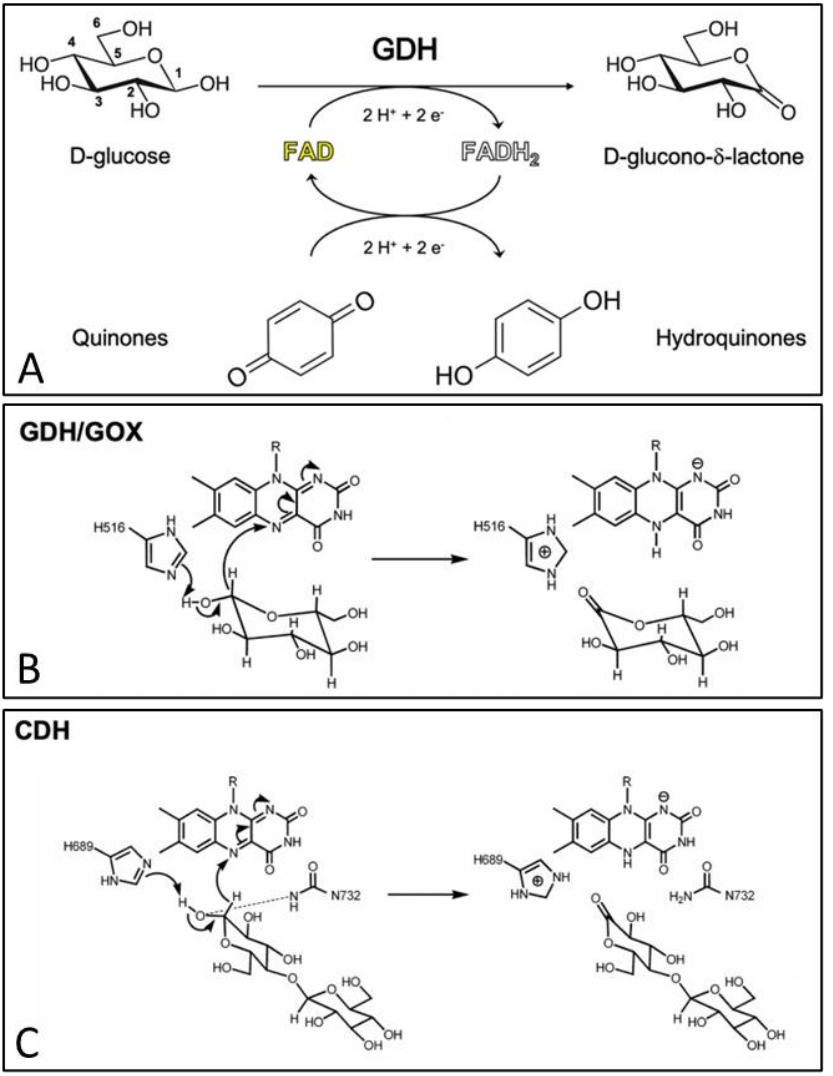

Figure 1.8 *(**A**) Catalytic cycle of GDHs. The cycle starts with the oxidation of the substrate (such as d-glucose) and the consequent reduction of the cofactor. In this phase, the cofactor in the oxidized state (FAD) is converted into the reduced state (FADH2), and D-glucono-δ-lactone is produced. In the second half-reaction, electrons are transferred from the reduced $FADH_2$ to electron acceptors, such as quinones. Proposed mechanisms of electron donor oxidation of GOX*[43]*, hypothesized also for GDH (**B**) and CDH*[39] *(**C**), in which His acts as a catalytic base*[37]*.*

Aim of the work

Role of a fungal enzyme couple in lignin degradation

The use of lignocellulose, and notably of residues from the wood, paper and agriculture sectors, is a field of intense study because plant biomass is a renewable source of polysaccharides and phenolic compounds. In perfect agreement with the principles of circular economy, lignocellulose-derived compounds have the potential to be used as molecules of industrial and pharmaceutical interest[44–46]. Lignin is the third most abundant biopolymer on earth, after cellulose, and it accounts for up to 30% of plant biomass[4]. It could be an inestimable source of aromatics of interest for organic syntheses, and probably the primary one after petrol runs out. However, its heterogeneous, randomly assembled and extremely complex chemical structure (which is fundamental for its protective role in the plant cell wall) makes its valorisation and exploitation scarce. A solution to this problem can be found in nature. In fact, filamentous fungi stood out as efficient degraders of lignin, shifting the attention of the scientific and industrial communities toward determining their mechanism of action. Their success is the result of a synergistic action of redox proteins, secreted by the fungus, that perform an enzymatic combustion[18]. These enzymes are mostly annotated within the "Auxiliary Activities" (AA) class defined in the Carbohydrate Active enZymes (CAZy) database[47]. The first step of lignin degradation is oxidative attack by lignin-modifying enzymes (LMEs), such as peroxidases (AA family 2, AA2) and laccases (AA1), which are subsequently supported by lignin-degrading auxiliary enzymes (LDAs)[8,17], encompassing the CAZy family AA3.

Attempts to simulate laccase-mediated lignin degradation *in vitro* showed that highly reactive radicals produced by laccase oxidation are prone to repolymerization into intermediates of higher molecular weight. This is one of the major obstacles in the exploitation of fungal laccases in industrial processes[48]. It is worth noting that these laccase-generated repolymerization products are even more recalcitrant to further enzymatic treatment owing to a net loss and gain in β-O-4 and C-C bonds, respectively. During *in vivo* degradation of lignin fungi

are able to prevent the massive repolymerization observed in *in vitro* studies, leading to the hypothesis that they possess mechanisms to control radicals produced during oxidative attack of lignin. A few studies have pointed out the possible role of AA3_2 enzymes in this event: the first on veratryl alcohol oxidase from *Pleurotus ostreatus*[49] and later glucose dehydrogenase (GDH) from *Glomerella cingulata*[50], as well as on oligosaccharide dehydrogenase (ODH)[29,51] and aryl alcohol dehydrogenases (AADs)[30] from *Pycnoporus cinnabarinus*. The current hypothesis predicts that these flavoenzymes use low-molecular-weight molecules, such as saccharides produced by enzymatic degradation of cellulose and hemicellulose, to fuel the reduction (inactivation towards re-polymerization) of phenoxy radicals deriving from laccase-mediated oxidation of lignin. To date, if the physiological role of AA3 enzymes is not fully understood, knowledge of their mechanisms of action, especially substrate specificity and the nature of their physiological electron acceptors, is limited. Recently, the three-dimensional structure of *Pc*ODH has unveiled the structural determinants responsible for substrate recognition and preferential activity towards different oligosaccharide electron donors[51].

This thesis aimed to analyse the interplay between laccase (*Pc*LAC) and oligosaccharide dehydrogenase (*Pc*ODH) from the fungus *Pycnoporus cinnabarinus*. Specifically, reproducing *in vitro* the *Pc*LAC oxidation on lignin-like-molecules and studying the effect of *Pc*ODH activity on the products of this reaction. Given the complexity of the lignin molecule, two model molecules (sinapic acid (SA) and guaiacol (GA)) were chosen to mimic some of the radical intermediates produced during lignin degradation.

The work is divided into two parts: the first focuses on the structural characterization of *Pc*ODH in complex with the two electron acceptor analogues; the second is the spectral characterization of *Pc*LAC oxidation reaction of SA and GA, in presence and absence of *Pc*ODH.

Materials and methods

3.1 Production of *Pc*ODH and *Pc*LAC

ODH and LAC from *P. cinnabarinus* (*Pc*ODH and *Pc*LAC) were expressed and purified at BBF (Marseille) in collaboration with Dr. Giuliano Sciara and Dr. Eric Record.
*Pc*ODH was recombinantly expressed in *Aspergillus niger* and purified on a Chelating Sepharose Fast Flow column (5 mL Ni Histrap, GE Healthcare, Velizy-Villacoublay, France) as previously described[29]. *Pc*LAC was expressed and purified from a monokaryotic strain of the fungus *Pycnoporus cinnabarinus* as described by Lomascolo et al.[52] .

3.2 Crystallization and crystal handling

Starting from the crystallization conditions of ligand-free *Pc*ODH obtained by Cerutti et al.[51], hand-made plates using the hanging-drop vapor diffusion method at 294 K were set up. Well-diffracting single crystals (***Figure 3.1***) were grown by mixing 1 μL of the protein solution and 1μL of the reservoir solution containing 2 M $(NH_4)_2SO_4$ and equilibrating the droplet against a reservoir solution (0.5 mL). Protein-SA complexes in the tetragonal (*Pc*ODH-SA*t*) and orthorhombic (*Pc*ODH-SA*o*) crystals were prepared by soaking ligand-free *Pc*ODH crystals in a solution containing 2M $LiSO_4$ and 2mM Sinapic acid (Sigma Aldrich) for 70 and 2.5 min respectively, by adding 5uL directly to the crystallization drop. Analogously, *Pc*ODH-GA crystals were obtained by 5 min soaking of *Pc*ODH native crystals in a solution containing 2M $LiSO_4$ and 20mM guaiacol (Sigma Aldrich). 2M $LiSO_4$ acted as the cryoprotectant Crystals were successively flash-frozen in liquid nitrogen and used for data collection at synchrotron radiation sources.

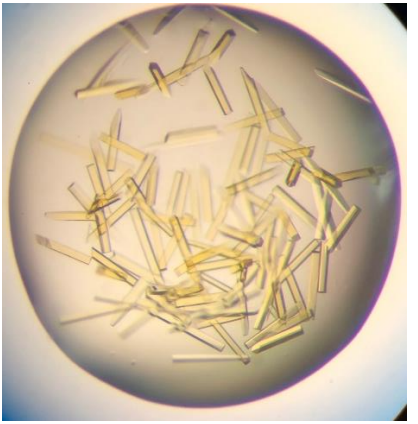

Figure 3.1 *Crystals of ligand-free PcODH. The oxidized FAD cofactor is responsible for the yellow colour to the crystals.*

3.3 Structure determination and refinement

X-ray diffraction data for *Pc*ODH-SA*t*, *Pc*ODH-SA*o*, and PcODH-GA were collected at the Soleil synchrotron (Saint-Aubin, France). All the datasets were collected at 100 K using a PILATUS detector. Data were indexed, scaled and integrated using the XDS package[53]. Molecular replacement was performed using MOLREP[54] from the CCP4 suite[55]. The ligand-free *Pc*ODH structure at 1.5 Å resolution[5] (PDB entry 6XUT) was used as the search model to calculate the initial crystallographic phases of *Pc*ODH-SA*t*, *Pc*ODH-SA*o* and PcODH-GA. Iterative automated and manual structure refinement were carried out using REFMAC5[56] and COOT[57], both implemented in the CCP4 suite. 5% of the reflections were excluded from refinement for cross validation by means of free R-factor. Manual adjustment was performed with the F_o-F_c map contoured at 3σ and the $2F_o$-F_c map at 1σ. Validation of the models, including Ramachandran statistics and B-factor analysis, was performed using the multimetric model geometry validation tool implemented in the CCP4 suite. Structural superposition was carried out using Superpose[58] implemented in the CCP4 suite. Figures were produced using Chimera[59].

3.4 Spectrophotometric studies: oxidation of sinapic acid and guaiacol

Laccase-mediated oxidation of Sinapic acid (SA) and Guaiacol (GA) was followed spectrophotometrically in 50mM citrate phosphate pH 4.5 buffer, at 30°C for 1h and 30minutes, respectively. SA and GA were dissolved in water at a maximum concentration of 2mM and added to the reaction to a final concentration of 0.5mM. The oxidation reaction with or without ODH (from 0.15 to 5.5nkat/mL, see ***Table 4.3***) was performed under the same experimental conditions, but with the addition of 500mM D-glucose. The reactions were started with the addition of *Pc*LAC and *Pc*ODH (in sequence) after 5min incubations of the enzyme-free reaction mixtures, to allow them to reach the desired temperature. Control reactions were performed in the same manner but without adding *Pc*ODH or D-glucose. To isolate one of the reaction intermediate, DAD, *Pc*LAC was deactivated, to stop the reaction by adding 1mM sodium azide[60] at the end of phase A, 7 min after the beginning of the oxidation reaction. The necessary azide concentration was chosen after preliminary test. After the addition of sodium azide, the reaction was monitored at 10°C and 30°C.
All reactions were carried out in 1mm quartz cuvettes and monitored with 1 min spaced acquisitions of UV/Vis absorption spectra collected between 190 and 1200 nm, using a spectrophotometer equipped with a photo diode array detector (Model 8453, Hewlet Packard).

3.5 Gas chromatography–mass spectrometry for identification of DAD

In order to analyse the intermediate produced at the end of *Pc*LAC phase A, 2.5nkat of the enzyme was incubated with 0.5mM of sinapic acid in 50mM citrate phosphate buffer pH 4.5 in a final volume of 5 ml. At the end of phase A, the reaction of laccase was stopped with 1mM NaAzide and stored at -80°C. A 0.5mL aliquot of the sample was acidified with 20µL of HCl (1M), extracted with 1mL of CH_2Cl_2

and 3mL of EtOAc and centrifuged for 15min. The organic phase was collected and dried under vacuum in a SpeedVac SC110 Savant (Thermo Fisher Scientific). The residue was dissolved in 30uL CH_2Cl_2 and 30uL of tert-butyldimethylsilyl chloride (TBDMS) were added as a derivatization reagent. The solution was heated for 1h at 353 K, dried under a stream of nitrogen and the residue was resuspended in 150μL CH_2Cl_2. 1μL of solution was directly injected in gas chromatography–mass spectrometry (GC-MS). GC-MS analyses were performed on a 6850A gas chromatograph (Agilent Technologies, Santa Clara, CA, USA) coupled to a 5973N quadrupole mass selective detector (Agilent Technologies). The carrier gas was helium at a constant flow of 1.0 ml/min. The ionizing energy was 70 eV (ion source 553 K; ion source vacuum 1025 Torr). Mass spectra were collected in the full-scan mode within them/z scan range of 50-800 atomic mass units.

Results

4.1 Structural features of *Pc*ODH in complex with electron acceptors

4.1.1 Overall structures

Soaking experiments with SA and GA were performed starting from ligand-free *Pc*ODH crystals. Three structures were solved: *Pc*ODH-SA*t* and *Pc*ODH-SA*o* in complex with sinapic acid, and *Pc*ODH-GA bound to guaiacol. The first belongs to the $P4_22_12$ space group (tetragonal) and contains two protein molecules in the asymmetric unit, whereas the other two belong to the $P2_12_12_1$ space group (orthorhombic), with one monomer in the asymmetric unit.
The final models of *Pc*ODH-SA*t*, *Pc*ODH-SA*o* and *Pc*ODH-GA were at 1.86 Å, 1.4 Å and 1.6 Å resolution respectively. Data collection and refinement statistics are summarized in ***Table 4.1***. The Ramachandran analysis indicates that for all three structures, most residues fall in the favoured region of 87.1% (SA*t*), 85.9% (SA*o*), and 96% (GA) with no outliers. The average Cα r.m.s.d values calculated for the superimposition of the three structures are shown in ***Table 4.2*** and confirm the presence of very little structural differences in the three structures. Only by observing the distribution of r.m.s.d values as a function of the residue number is it possible to detect a displacement of Cα atoms exceeding 10 Å in the B13-B14 loop. This region, known as the "substrate binding loop"[51], is exposed to the solvent environment in *Pc*ODH-SA*o* and *Pc*ODH-GA structures, while undergoing a movement of 17 Å toward the active site in *Pc*ODH-SA*t*.
The overall structures of *Pc*ODH in complex with the two electron acceptor analogues, share the fold of the GMC superfamily typically composed of two major structural domains: a N-terminal FAD binding domain and C-terminal a substrate binding domain[5] (***Figure 4.1***).
As already described by Cerutti et al.[51], the flavin-binding domain is composed of five-stranded parallel β-sheet A (B1, B2, B6, B10, B18)

***Table 4.1**: Data collection and refinements statistics. Values in parentheses are for the highest resolution shell.*

	*Pc*ODH-SA*t*	*Pc*ODH-SAo	*Pc*ODH-GA
Data collection			
Space Group	$P4_22_12$	$P2_12_12_1$	$P2_12_12_1$
Unit-cell dimensions (Å)	a= 147.53	a=49.14	a=48.88
	b=147.53	b=61.8	b=61.51
	c=142.79	c=195.99	c=195.14
Resolution range (Å)	49.18- 1.86 (1.89-1.86)	49.00-1.40 (1.42-1.40)	47.46-1.60 (1.63-1.60)
Number of observations	3639248 (184551)	1595497 (78022)	1010890 (53238)
Unique reflections	131815 (6475)	118712 (5744)	78710 (3888)
Completeness (%)	100 (100)	100 (100)	99.9 (99.7)
Redundancy	27.60 (28.50)	13.40 (13.60)	12.8 (13.7)
I/σ (I)	8.4 (0.8)	10.0 (0.7)	14.5 (1.7)
R_{merge} [a] (%)	0.499 (9.215)	0.105 (3.187)	0.083 (1.61)
$CC_{1/2}$	96.7(36)	99.9 (42.3)	99.9 (16.5)
Wilson B-value ($Å^2$)	25.32	27.23	28.84
Refinement			
Resolution range (Å)	49.042-1.86	49.04/1.40	47.46-1.6
Molecules per asymmetric Unit	2	1	1
R_{work}/R_{free} [b]	0.1564/0.1916	0.1712/0.2307	0.1719/0.2101
Real-space corr coefficients	0.21	0.38	0.34
Deviation from ideal geometry			
Bond (Å)	0.0103	0.139	0.012
Angles (°)	1.6682	0.885	1.766
Ramachandran plot (%)			
Favoured/Allowed/outliers	87.1/13.1/0	85.9/14.1/0	96/4/0
Mean B-factors ($Å^2$)			
Protein	25.11	32.37	30.08
FAD/SA/GA	17.65/60.10/ -	23.00/33.75/-	22.00/-/43.70
Water/Sulphate	36.68/59.76	64.79/39.80	30.10/59.70
Number of atoms			
Protein	9930	5393	5313
FAD/SA/GA	53/112/-	53/32/-	53/-/18
Water/Sulfate	1146/100	546/40	310/40

a. $R_{merge} = \sum_i \sum_j | I_{i,j} - \langle I_j \rangle | / \sum_i \sum_j I_{i,j}$, where i runs over multiple observations of the same intensity, and j runs over all crystallographically unique intensities.

b. $R_{work} = \sum \big| |F_{obs}| - |F_{calc}| \big| / \sum |F_{obs}| / \sum_i \sum_j I_{i,j}$, where $|F_{obs}|>0$. R_{free} is based on 5% of the data randomly selected and is not used in the refinement.

positioned between three-stranded antiparallel β-sheet B (B7, B8, B9) and three α-helices (H1, H9, H20). B1, H1, and B2 form the βαβ motif involved in the stabilization of the FAD cofactor.

***Table 4.2**: Cα r.m.s.d values calculated for the superposition of structures PcODH-SAt, PcODH_SAo, PcODH-GA using Superpose*[58]

	***Pc*ODH-SAt**	***Pc*ODH-SAo**	***Pc*ODH-GA**
***Pc*ODH-SAt**	-	0.264	0.153
PcODH_SAo	0.264	-	0.158
***Pc*ODH-GA**	0.158	0.153	-

The substrate-binding domain consists of the central six-stranded antiparallel β-sheet C (B5, B11, B12 B17), supported by seven α-helices (H8, H12, H13, H14, H15, H17, H18).
Three potential N-glycosylation sites (Asn38, Asn188, and Asn439) in the amino acid sequence of ODH were predicted using the consensus sequence Asn-X-Ser/Tr. All three N-glycosylations were visible in the structures. The Asn439 sites show the longest well-defined electron density, with two β(1-4) linked N-acetylglucosamines and a β(1-4) linked mannose. In the case of Asn38 and Asn188, the first N-acetylglucosamine showed a defined electron density in the *Pc*ODH-SA*t* structure, whereas in the other structures a less clear density is attributable to the first NAG.
The overall electron density is of high quality except for the region composed of beta strand B1, Helix H1 and B2 (residues 20-50), and between residues 230-300, the one connecting β-strands B8 and B9 (residues 269-275). In these regions, the electron density is discontinuous in both *Pc*ODH-SA*o* and *Pc*ODH-GA structures.

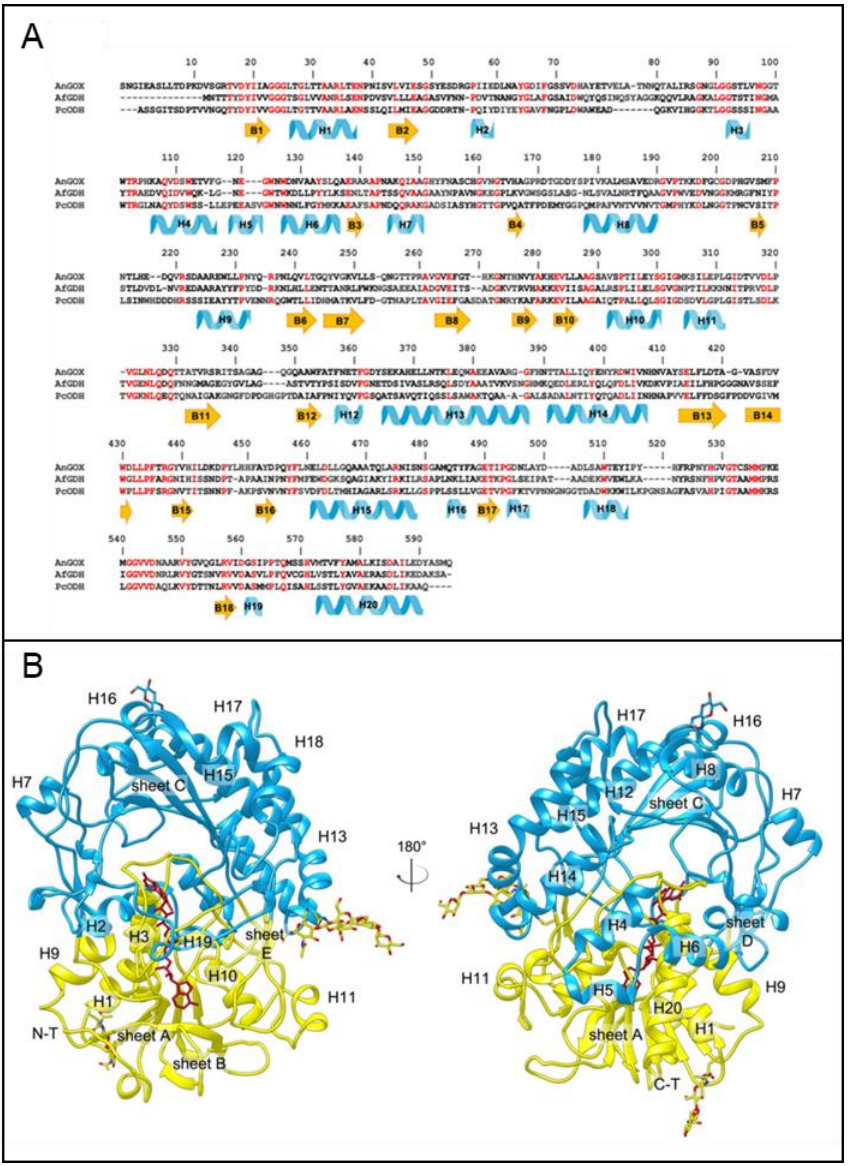

Figure 4.1 *Overall structure of PcODH and sequence alignment with homologous enzymes of known structure (AfGDH, AnGOX) based on structural superposition (**A**). Structure of ligand-free ODH: in yellow the FAD-binding, in blue the substrate-binding domain, FAD in red* [51] *(**B**).*

4.1.2 PcODH-SAt structure

*Pc*ODH_SA*t* belongs to the $P4_22_12$ space group with a dimer in the asymmetric unit. The interaction of the monomers occurs at the interface of the convex face (monomer B) and concave face (monomer A). Analysis of the structure using the online software PISA (Protein Interfaces, Surfaces and Assemblies)[61] suggests that this interface does not play any role in complex formation and seems to be a result of crystal packing only. A total of seven SAs are present in the structure: two in each active site, one on the external surface of monomer A, and two in the interface between the two monomers that compose the asymmetric unit (***Figure 4.2***). The overall architecture of ligand-free *Pc*ODH is conserved in *Pc*ODH_SA*t* and r.m.s.d average value calculated on the superimposition of the Cα atoms is 0.226. Despite a low average r.m.s.d, there is a 10 Å displacement of Cα atoms in the region of the B13-B14 loop (known as the "substrate-binding loop" which comprehends residues 419-424) (***Figure 4.3***). As already seen in the structures of *Pc*ODH in complex with electron donors[51] this loop is locked in a conformation that restricts access to the active site instead of pointing toward the solvent, as in ligand-free ODH. This displacement occurs upon sugar-binding in the active site. In the equivalent position, we find SA in *Pc*ODH-SAt crystals, although in this case the binding loop closure seems to be imposed by crystal packing (***Figure 4.3***). This result is compatible with the high flexibility of the B13-B14 loop. In this case, the movement of the B13-B14 loop toward the solvent is prevented by the presence of residues belonging to H6, B3, H7, and B4 from the other enzyme monomer present in the asymmetric unit.

It is interesting that the ligand-free *Pc*ODH crystals belong to an orthorhombic space group, while *Pc*ODH-Sa*t* crystals belong to the orthorhombic one. Considering that the transition to another group space with a monomer in the asymmetric unit would cause damage to the crystal during soaking, a change in space group after soaking with sinapic acid has been discarded, and polymorphism in the drop has been hypothesized. In fact, the symmetry axis that relates monomer A to monomer B in the tetragonal space group does not coincide with

any of the three symmetry axes of the Orthorhombic Group. This suggests that crystals with tetragonal and orthorhombic space groups were present simultaneously, probably with the orthorhombic space group being the majority. In monomer A, there are three SA molecules. bound: two, SA*t*1 and SA*t*2, are in the active site, close to the FAD cofactor and the substrate binding loop respectively; the other is at the interface with the symmetry-related monomers (SA*t*4). It is stabilized by H-bonds with Asn55 and Asp52 of the ODH concave surface and with two water molecules found at the interface, one of which connects it to Lys588 from monomer B of the asymmetric unit (***Figure 4.2 C)***. SA*t*4 is the most distant from the edge of the funnel-shaped cavity leading to the active site. In the case of monomer B, the positions of these three synapic acids are conserved (SAt1, SAt2, SAt4) but SAt4 loses the direct contact with Asn55 and Asp52 which is now mediated by a water molecule; moreover, there is a fourth synaptic acid molecule (SA*t*3, occupancy=0.75) bound halfway between SAt4 and SAt2 (***Figure 4.2 B***). The position of this fourth molecule suggests a diffusion path: it is located at the edge of the cavity connecting the two sinapic acids in the active site and the distant one on the surface. Although access to the active site is positioned at the interface between monomers A and B, there is still enough space to allow the passage of these molecules and get to the active site, creating what looks like a diffusion route, (***Figure 4.2 A)***. The first sinapic acid molecule in the active sites of both monomers (SA*t*1) is positioned at the bottom of the substrate-binding cavity, with its carboxyl group facing the cofactor and the aromatic ring in the opposite direction. The carboxyl group forms hydrogen bonds with two catalytic histidines (Nδ1-H571 and Nε2-His528), the FAD N5 reactive atom and with Val526 backbone through a water molecule (***Figure 4.4)***. The methoxy oxygen (-OCH_3) in the aromatic ring is hydrogen-bonded to Gly98 and Ile61 through two water molecules. The two synapic acids in the active site, SA*t*1 and SA*t*2, are oriented so that the aromatic rings are adjacent to each other (packed around Tyr64), and the carboxyl tail of SA*t*2 forms hydrogen bonds with SA*t*1 phenol. This OH group is connected to Asp418, which forms two H-bonds with the carbonyl of SA*t*2.

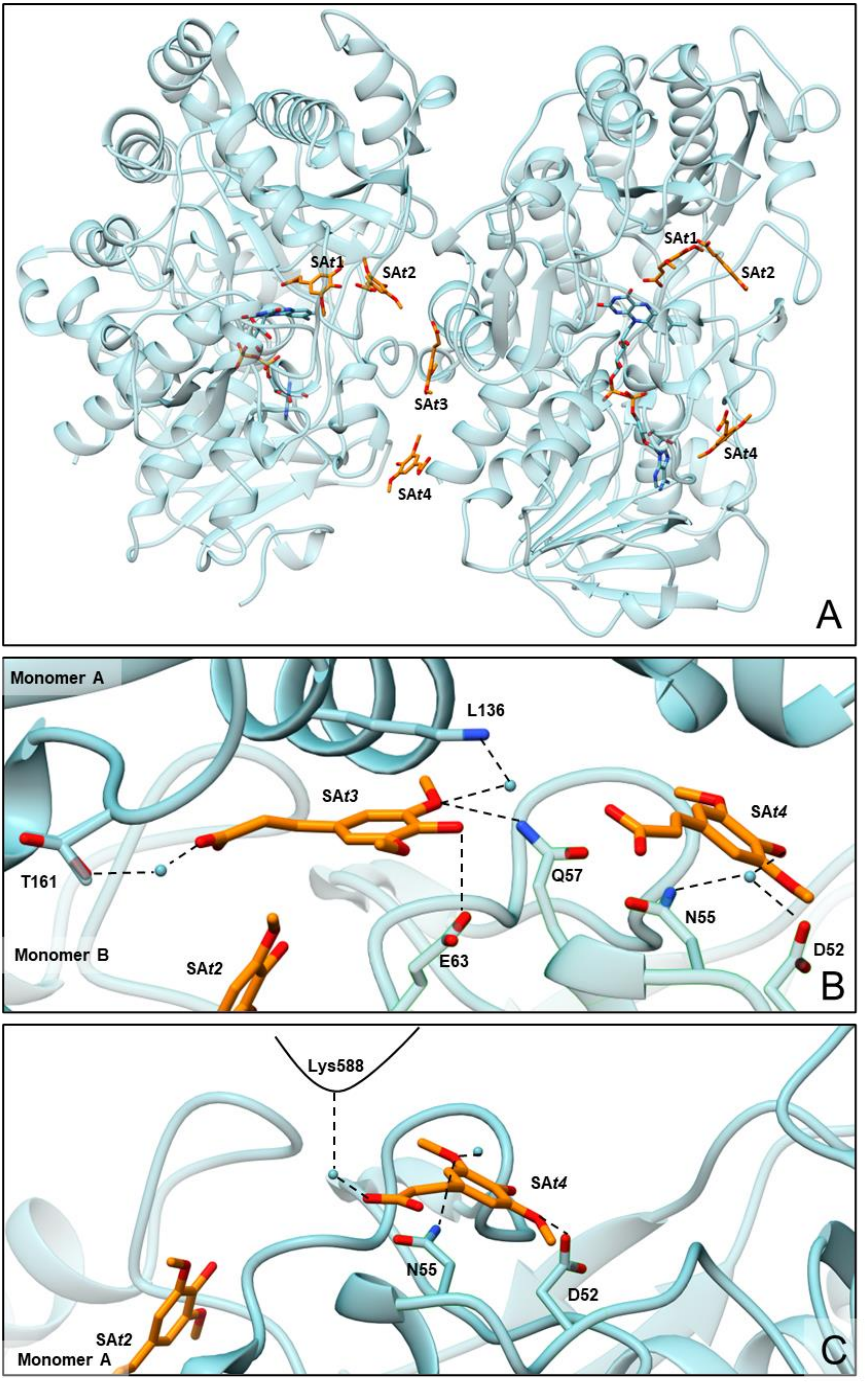
SAt1
SAt2
SAt3
SAt4
SAt1
SAt2
SAt4
A
Monomer A
L136
SAt3
SAt4
T161
Q57
N55
Monomer B
SAt2
E63
D52
B
Lys588
SAt4
N55
D52
SAt2
Monomer A
C

Figure 4.2 *Overall three-dimensional structure of PcODH-SAt and sinapic acids present at the interface of monomer A and B. Sinapic acids are in orange sticks. The three SA (SAt1, SAt2, SAt3, named after the distance from the FAD) share the same position, and the fourth which is located further from the active site, is only present in monomer A. Their position suggests a diffusion pathway from the solvent environment to the flavin system.*

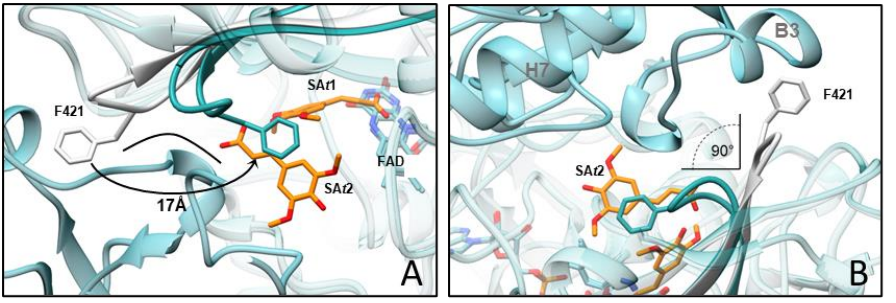

Figure 4.3 *Superposition of ligand-free PcODH (gray) and PcODH-SAt (cyan) structures; sinapic acids molecules are coloured in orange, by etheroatom. Panel A and panel B represent different views.*

Since this molecule is at the edge of the active site, it interacts with a water molecule, which in turn is bonded with Lys133 of a symmetry-related molecule.
Both sinapic acids are stabilized by π–π stacking interactions[62–64] with the aromatic residues that face the active site. Notably, Phe421 (from the substrate binding loop) and Phe416, that also bind saccharide electron donors and that packs all ligands around Tyr64.

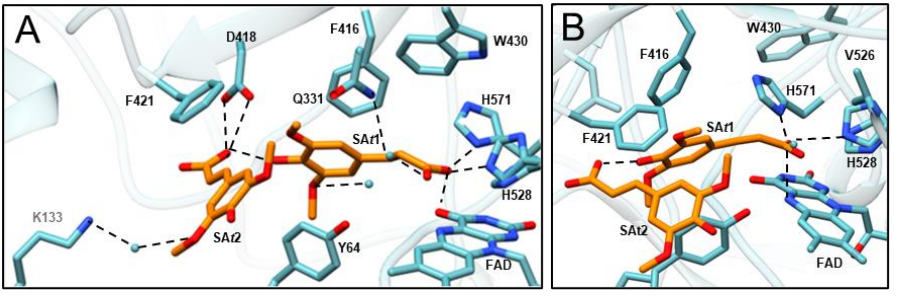

Figure 4.4 *Superposition of ligand-free PcODH (gray) and PcODH-Sat (cyan) structures; sinapic acids molecules are coloured in orange, by etheroatom. Panel A and panel B represent different views of monomers A active site. Residues are conserved in monomer B.*

4.1.3 PcODH-SAo and PcODH-GA structures

*Pc*ODH-SAo and *Pc*ODH-GA belong to the $P2_12_12_1$ space group with only one monomer in the asymmetric unit. The same space group characterized crystals corresponding to ligand-free, GLC-bound and LMB-bound *Pc*ODH structures. Two SA and two GA are present in the two structures: one ligand is in the active sites and the other is on the external surfaces of the proteins (***Figure 4.5 A, B***). Both structures preserve the architecture of ligand-free *Pc*ODH and the r.m.s.d average values calculate on the superimposition of the Cα atoms are 0.141 and 0.158 for *Pc*ODH_SA*o* and *Pc*ODH-GA, respectively.
They present an open conformation in which the substrate-binding loop does not restrict access to the active site of the protein (***Figure 4.5 A, B***): in fact, Phe421 faces the solvent. The mobility of this B13-B14 loop required the modelling of two conformations, which still left the substrate cavity open.
SA*o*2 and GA2, which are positioned on the surface of ODH, are stabilized by π–π stacking and CH-π interactions with His346 and Phe421 respectively. SA*o*2 is dragged slightly more toward the active site (~1.6Å) than GA2, because of the interaction of carboxyl with NH of Phe421 backbone (***Figure 4.5 C, D, E, F***).
There is only one sinapic acid (SA*o*1) and one guaiacol (GA1) inside the active sites of the two structures, close to the FAD ring, in the analogous position of what observed for SA*t*1. However, unlike SA*t*1 and SA*o*1, whose carboxyl group binds catalytic histidines and FAD, GA1 does not participate in any hydrogen bond with the protein environment: but its aromatic ring is engaged in π–π stacking interactions with Phe416 and Tyr64 (***Figure 4.5 F***), like for the SA*o*1 ligands. Beyond these aromatic interactions, SA*o*1 is engaged in carboxyl group-mediated hydrogen bonds with His528, His571 and FAD N5, as previously described for SAt1, and with Val526 and Gln331 through a water molecule. The methoxy oxygen (-OCH_3) of the aromatic ring is connected to Thr349 by an H-bond with a water molecule (***Figure 4.5 F***).

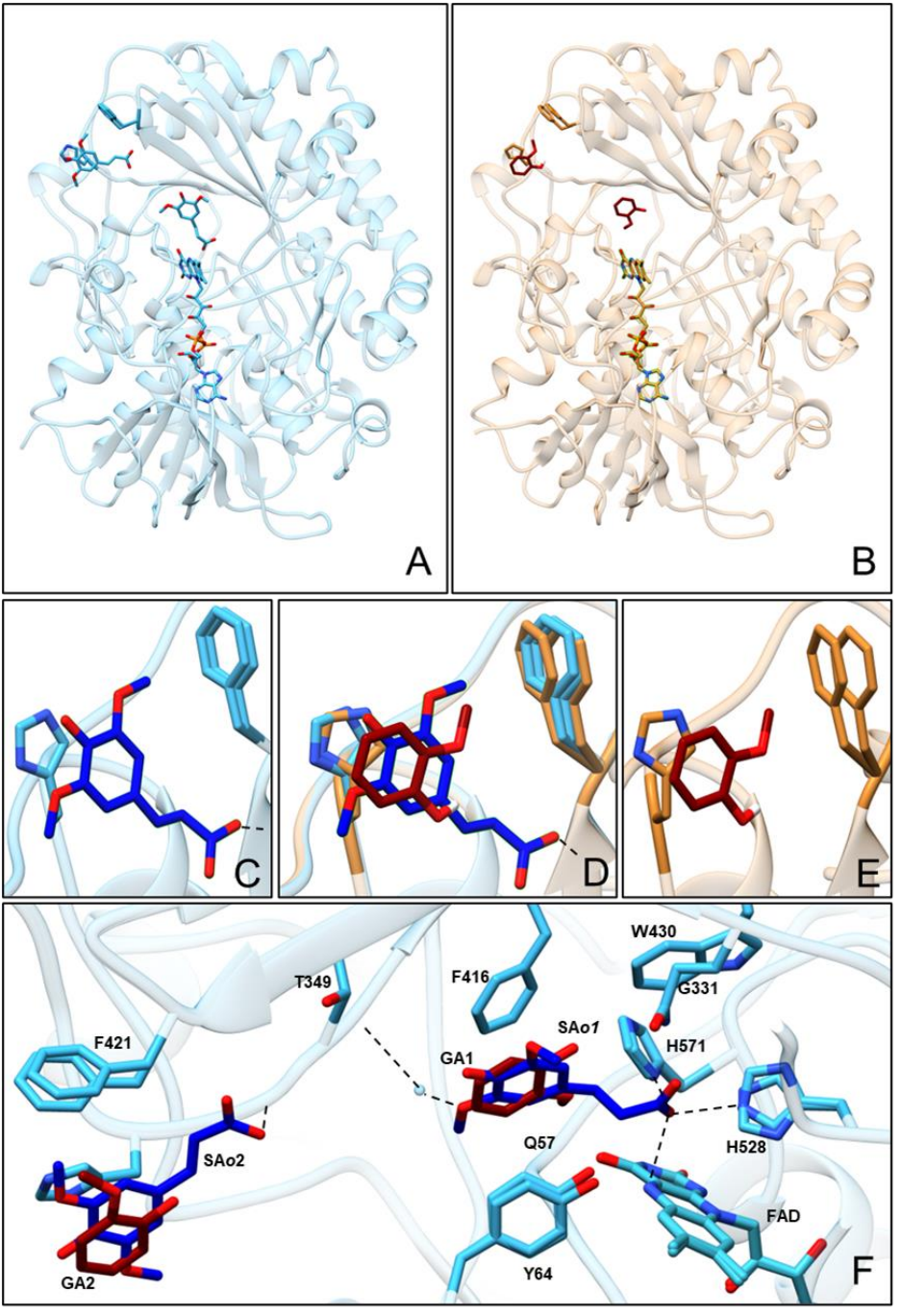
A
B
C
D
E
W430
T349
F416
G331
F421
SAo1
H571
GA1
SAo2
Q57
H528
FAD
Y64
GA2
F

Figure 4.5 *Overall three-dimensional structure of PcODH-SAo (light blue, **A**) and PcODH-GA (light brown, **B**); Sinapic acids are on blue sticks and guaiacols are in dark red sticks. Details of the binding of SAo2 (**C**) and GA2 (**E**) with His346 and Phe421 and their superposition (**D**). Panel **F** represents the superposition of PcODH-SAo and PcODH-GA in the active site: aromatic rings of GA1 and SAo1 share the same position and π–π stacking interactions.*

4.1.4 Superimposition of structures bound to electron acceptors

As noted in all structures of *Pc*ODH, no major conformational change is observed for residues that directly face the active site, apart from the substrate-binding loop, whose conformation in PcODH-SA*t*1 is determined by crystal packing. Small differences can be found in the network of interactions of the ligands.

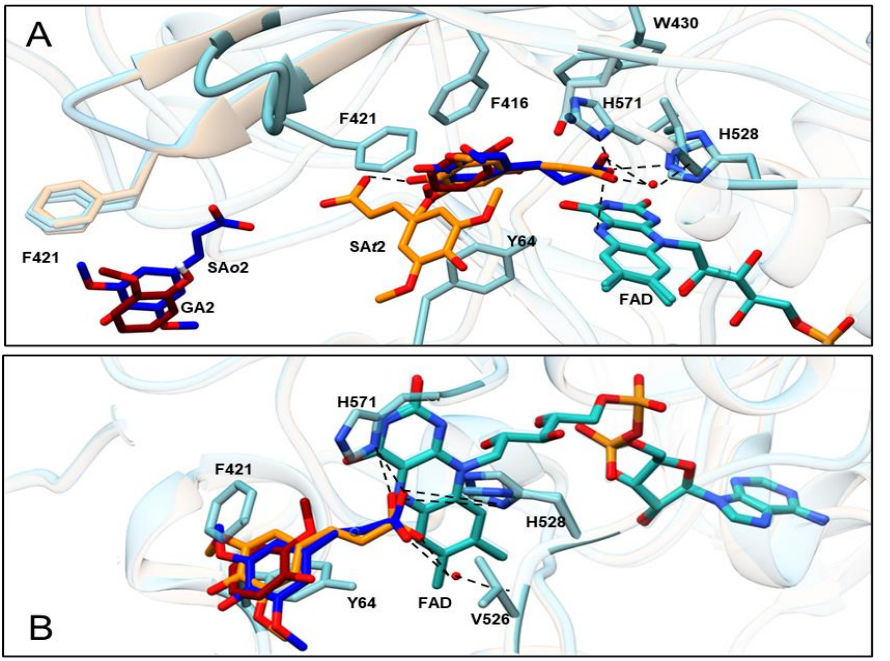

Figure 4.6 *Superposition of PcODH-SAt (cyan), PcODH-SAo (light blue) and PcODH-GA (light brown). Detail of the active site. SAo2 and SAo1 are in orange sticks, SAt1 and SAt2 are in blue sticks, Ga1 and Ga2 are in dark red sticks. GA1, SAo1 and SAt1 share the same position in the active site.*

Interestingly, SA*t*1, SA*o*1 and GA occupy equivalent positions within PcODH active site. Their aromatic rings are engaged in π-π stacking interactions with the same residues, Phe416, Tyr64, which stabilize these molecules and impose strict directionality. The long carbon chains of both sinapic acids (SA*t*1 and SA*o*1) are similarly involved in H-bonds with His528, His571 and the reactive N5 of FAD, and with Gln331 and Val526 through water (***Figure 4.6***). A stereo view of the Fo-Fc electron density of ligands in the active site of the three strucrures is visible in ***Figure 4.7***.

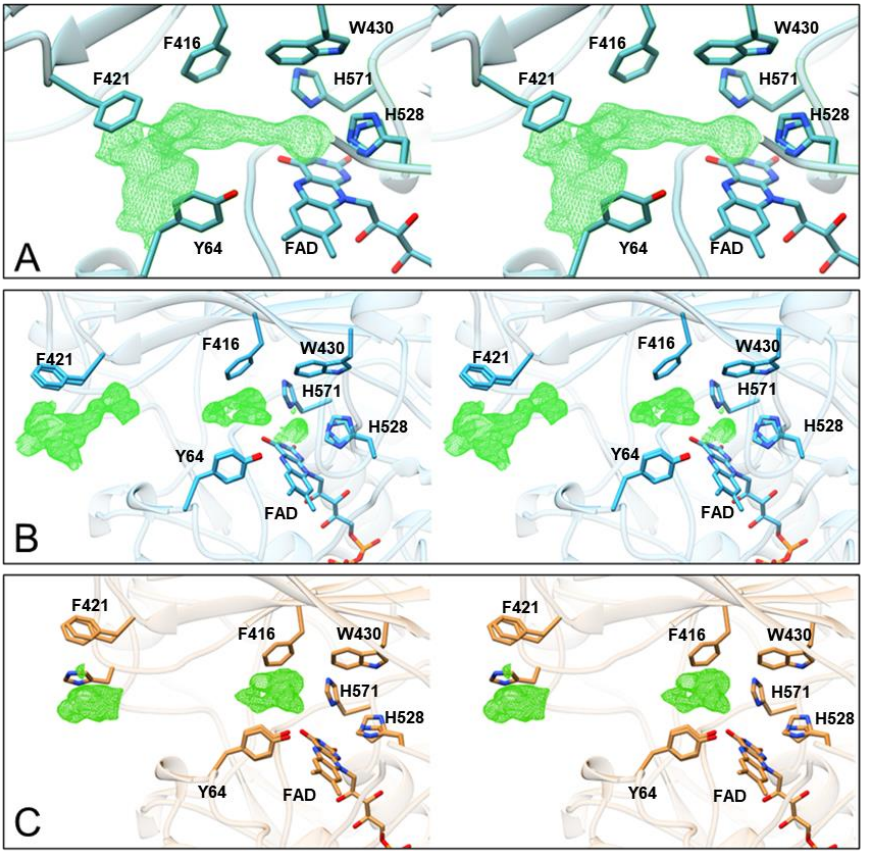

Figure 4.7 *Stereo view of the Fo-Fc electron density of ligands, contoured 3σ. (**A**) SAt1 and SAt2 in active site of PcODH-SAt; (**B**) SAo1 and SAo2 in active site of PcODH-SAo; (**C**) GA1 and GA2 in active site of PcODH-GA.*

4.2 Comparison with structures of *Pc*ODH in complex with electron donors

4.2.1 Overall structures and active sites

Structures of *Pc*ODH in complex with electron donors have been previously solved, *i.e.* bound to glucose (ODH-GLC, PDB entry 6XUU) and laminaribiose (ODH-G3G, PDB entry 6XUV)[51]. Structures will be compared as follows, based on the number of ligands found in the active site: PcODH_SA*t* (two SA molecules in the active site) will be compared to *Pc*ODH-G3G (bound to laminaribiose, (a molecule of two units of connected by a β1-3 glucose dimer); *PcODH_SAo* and *Pc*ODH-GA (one molecule in the active site) will instead be compared to *Pc*ODH-GLC (bound to glucose).
The first visible difference between the *Pc*ODH-GLC and *Pc*ODH_SA*o* /GA is the movement of the B13-B14 loop: in the first structure the binding of two molecules of glucose causes the movement of the Phe421 from facing the solvent to moving inside the active site. The presence of the second glucose (the non-reducing one), that interacts with Phe421, induces this rearrangement of the substrate binding loop. Despite the presence of a ligand in the active site, ODH-SAo and ODH-GA show an open conformation of the substrate binding loop. Indeed, in this conformation, Phe421, faces the solvent environment, yet still interacts with a second molecule of sinapic acid or guaiacol (SA*o*2 and GA2), also bound by His346. The aromatic ring of these molecules is engaged in parallel and perpendicular π-π staking with His346 and Phe421, respectively. No electron acceptor is found in the position of non-reactive GLC2, held in place in *Pc*ODH-GLC by Phe421, allowed by a "close" substrate binding loop conformation. Inside the active site, the aromatic rings of SA*o*1 and GA1 occupy similar positions as the reactive glucose. However, their position is more similar to that of the α glucose anomer rather than the β anomer: the aromatic ring is shifted 2 Å and 3.8 Å from the position of the α and β anomer, respectively. This suggests that the contribution to the binding of the aromatic ligand moieties is rather provided by Phe421

and Tyr64 than by Trp430, which plays a more important role in binding glucose, especially the reactive β anomer, ***Figure 4.8 A, B***).
Unlike guaiacol, the carboxyl group of SA*o*1 interacts with His528 and with FAD reactive N5, like glucose reactive hydroxyl, and with His571. This position is compatible with proton abstraction by His528, as hypothesized in a catalytic mechanism that relies on hydride transfer. However, it should be noticed that sinapic acid is neither an electron acceptor nor an electron donor for *Pc*ODH, although its radical form is (see functional results). Finally, the carboxylic tail of sinapic acid binds through water to Val526, the same residue that glucose O2 hydroxyl binds in *Pc*ODH-GLC.
Comparing *Pc*ODH-SA*t* to *Pc*ODH-G3G, we notice that the two SA molecules occupy equivalent positions than the two laminaribiose glycosyl units, stabilized by aromatic stacking with Phe416 and Tyr64 (SA*t*1) and with Phe421 and Tryr64 (SA*t*2).
As for SAo1, the long carboxyl chain of SAt1 allows it to establish hydrogen bonds with both catalytic histidines and the FAD cofactor, unlike the reducing unit of laminaribiose that only interacts with His528 and FAD (***Figure 4.8 C, D)***.
The interactions of ligands with the protein active site environment show minor differences: SA1 shifted position caused the loss of direct interactions of laminaribiose with Val526 and Gln331 are lost in SAt1 and SAo1, shifted and bridgeed to Val526 by water molecule. The bond between glucose O6 hydroxyl and the FAD cofactor is also lost in SAt1 and SAo1.

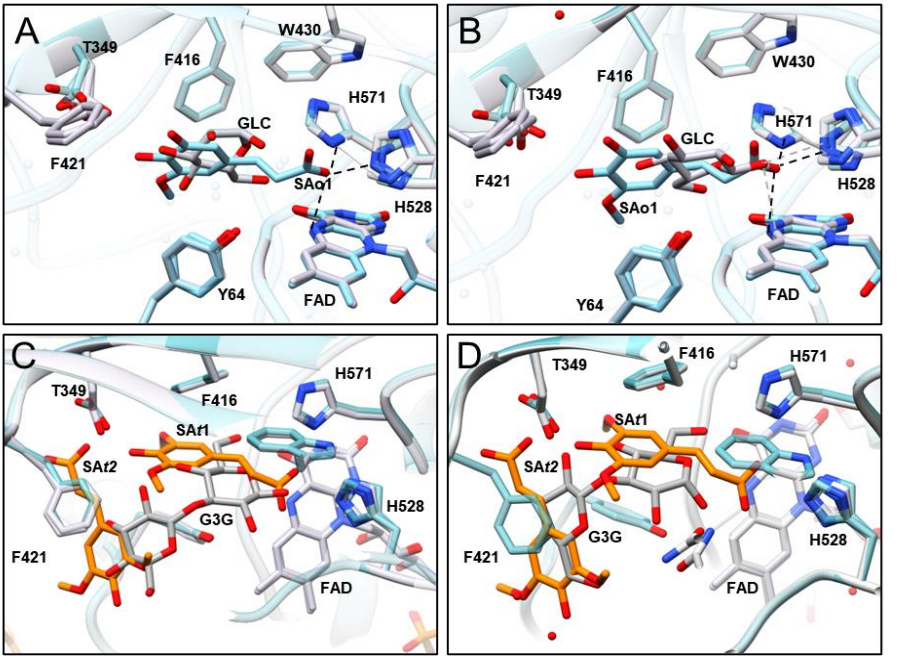

Figure 4.8 *Comparison with structures of PcODH in complex with electron donors; superposition of PcODH-SAo (light blue) with PcODH-GLC (light grey) with detail of anomer α of glucose (**A**) and anomer β (**B**); superposition of PcODH-SAt (cyan, SAt1 is in orange sticks) with PcODH-G3G (grey) with detail of anomer α of laminaribiose (**C**) and anomer β (**D**).*

4.2.2 FAD geometry with electron acceptors

The FAD molecule of *Pc*ODH-SA*t*, *Pc*ODH-SAo and *Pc*ODH-GA show an almost planar conformation (***Figure 4.9 B, D, F),*** with an angle between the pyrimidine and dimethylbenzene rings of 163.65°, suggesting that the FAD cofactor is in the oxidized state[65]. This is in accordance with the nature of the ligands used, SA and GA, that neither act as electron donors nor as electron acceptors. We will show in fact in the functional results section that they act as electron acceptors once activated in their oxidized radical form.

The structures of *Pc*ODH bound to electron donors (glucose, laminaribiose) showed instead a pronounced distortion from planarity (***Figure 4.9 E)***. This was expected since saccharides act as electron donors and bring the FAD to its a reduced state. In the case of PcODH-GLC and PcODH-G3G, electron density didn't allow modelling a totally reduced (bent) FAD moiety, but only an intermediate conformation between bent and planar. In this state the pyrimidine moiety was 11° more bent toward the FAD-binding domain, with respect to the pteridine plane, than in the oxidized form. Distortion from planarity of the oxidized FAD cofactor has been already observed for other GMC oxidoreductases, in which a conserved asparagine causes a distortion of the isoalloxazine ring[43,65,66]. Conserved in *Pc*ODH (Asn97), this residue establishes hydrogen bonds with Ser573, the FAD and ODH backbone (not shown in figure). FAD pyrimidine moiety is also hydrogen bonded to Ala99 and Ala100[5], and FAD N5 to Gly98 (***Figure 4.9 A)***. In the case of glucose- or laminaribiose-bound structures, this bond is missing (the distance in both cases is 3.99 Å), as a result of extra FAD bending upon oxidation (***Figure 4.9 C)***. In *Pc*ODH structures with the electron acceptor analogues SA and GA, the distance between FAD N5 and Gly98 is again compatible with H-bonds (3.05 and 3.09 Å, respectively), as in the the oxidized, ligand-free form.

4.2.3 External sugar-binding sites

A peculiar feature observed in sugar-bound *Pc*ODH structures (*Pc*ODH-GLC and *Pc*ODH-G3G) is the presence of three sugar-binding sites (SBSs) on the surface of the protein, distant from the active site entrance, on the concave enzyme side[51]. The molecular bases for binding recognition at these sites seems to be limited to sugars, as no SA or GA have been found in these pockets in the three structures analysed in this work. As such, these SBSs might be specific for saccharides and possibly allow anchoring to polysaccharide domains within lignocellulose during fungal lignocellulolytic activity.

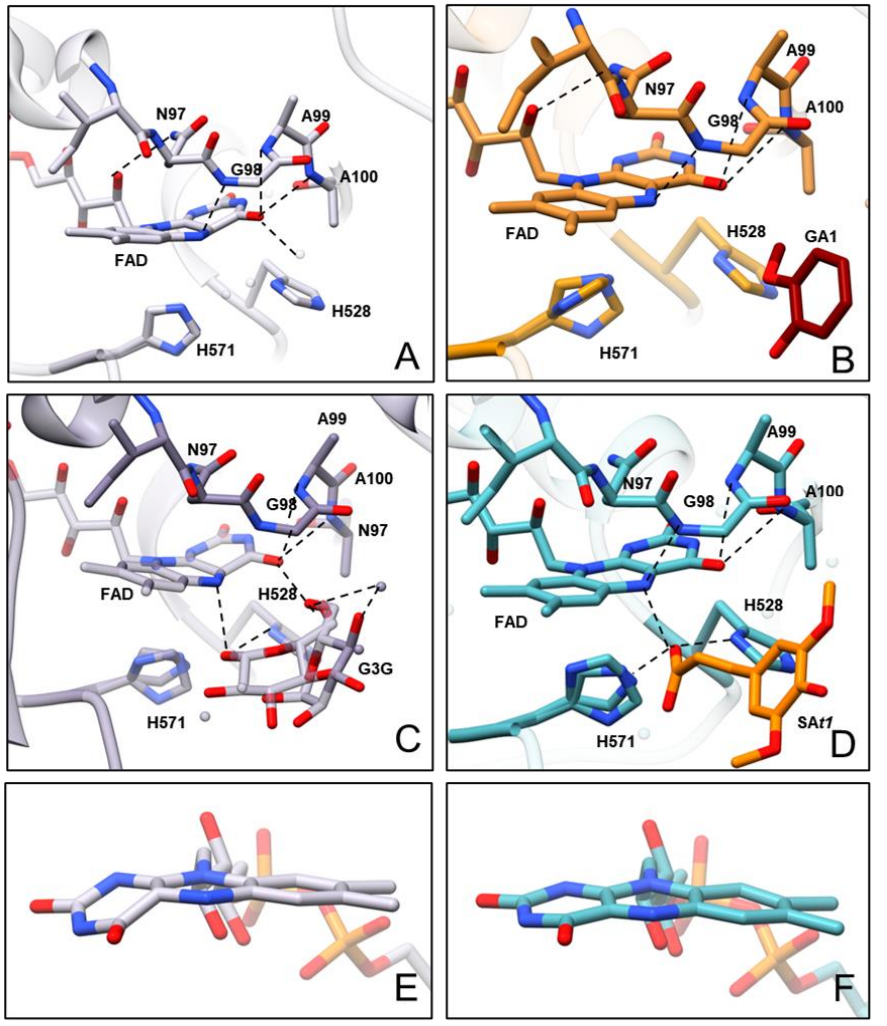

Figure 4.9 *FAD geometry with electron acceptors; details of Gly98 interaction with FAD in PcODH-ligand free (**A**), PcODH-GA(**B**), PcODH-G3G (**C**), PcODH-SAt (**D**); (**E**) PcODH bound to electron donor (PcODH-G3G) show a clear distortion from planarity in particular the pyrimidine moiety is 11° bent toward the FAD-binding domain with respect to the pteridine plane; (**F**) the FAD molecule of PcODH-SAt, shows a planar conformation with an angle between the pyrimidine and dimethylbenzene ring of 163.65°.*

4.3 Functional characterization of enzymatic reactions with Sinapic acid and guaiacol

4.3.1 Reaction of PcLAC with Sinapic acid

The oxidative reaction of sinapic acid by laccase from *P. cinnabarinus* (*Pc*LAC) was studied spectrophotometrically, following changes in the UV-visible spectra. The spectral changes of the reaction mixture of *Pc*LAC and sinapic acid are shown in ***Figure 4.10 A***. The enzymatic transformation of SA by *Pc*LAC, resembles the oxidation of sinapic acid by Polyphenol Oxidases from *Trametes Versicolor*, described by Lacki and Duvniak[67]. It is a multiphase reaction composed of two phases. Phase A starts with the addition of *Pc*LAC in a reaction mixture composed of sinapic acid in buffer 50mM citric acid pH 4.5 (blue absorption spectrum in ***Figure 4.10 B***). Consumption of SA can be considered as the end of phase A and the beginning of phase B. During phase A, the oxidation of sinapic acid results in a relatively rapid decrease in its absorbance peaks at 233 and 315nm, with a simultaneous increase in a peak at 208 nm (***Figure 4.10 C***). The reaction intermediate responsible for this peak (green absorption spectrum in ***Figure 4.10 B***) was identified as dehydrodisinapic acid dilactone (DAD) by FTIR, NMR and Mass Spectrometry[67]. An isosbestic point at 219 nm indicates that SA is converted into DAD without detectable accumulation of any other intermediate. During phase A the reaction solution remains colourless. During phase B instead, enzymatic consumption of DAD occurs and additional products are formed, corresponding to decrease in the peak at 208 nm followed by a rapid reddish response, with broad absorbance between 470 and 515nm (***Figure 4.10 D***). At the end of phase B, the colour of the reaction becomes dark red. The presence of an isosbestic point at 259nm suggests that DAD is converted into the final reaction intermediates and products while enzymatic oxidation proceeds. ***Figure 5.1*** **A** shows a scheme of the reaction pathway of the oxidation of SA[67–69]. According to Lacki et al.[67], the reaction path of SA oxidation is a combination of enzymatic and non-enzymatic reactions.

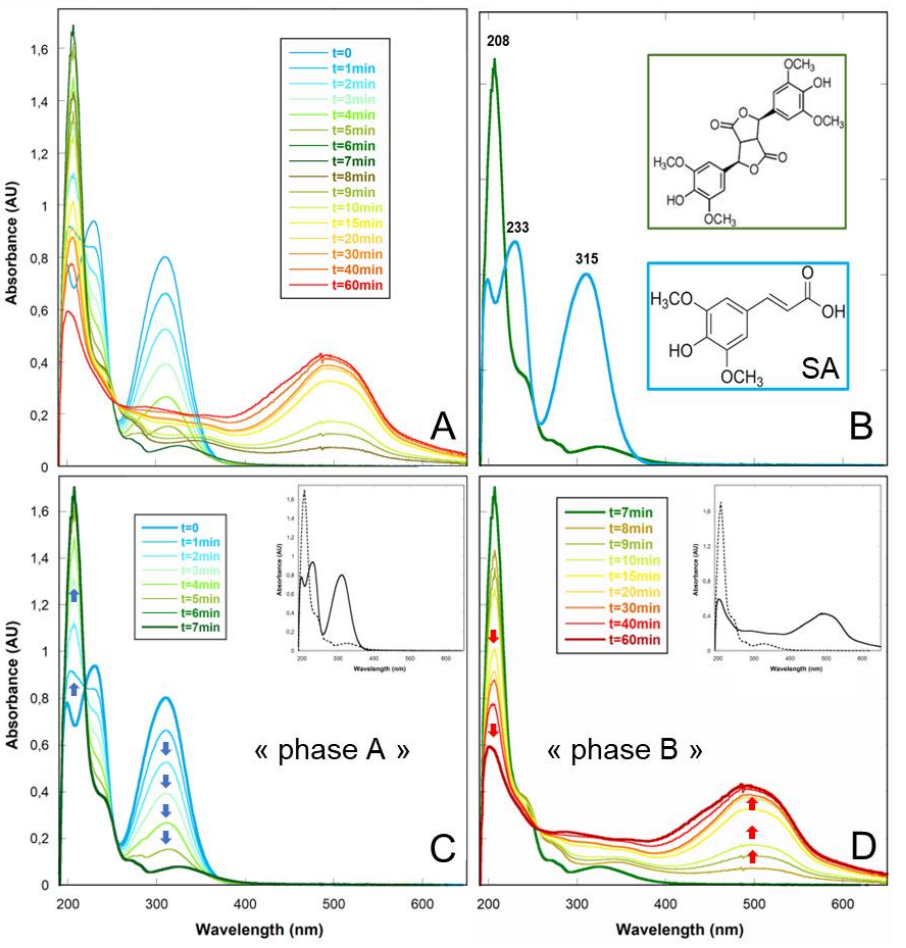

Figure 4.10 *Changes in the UV-Vis spectra of Rx4 of Table 4.1. The entire reaction (1h) is shown (**A**). Each line represents a different time of the reaction (see legends). The entire reaction has been devided in phase A (**C**) phase B (**D**). Inserts show the visible initial spectra (continuous line) and final spectra of phase A and phase B(dashed lies). For visual clarity and continuity, the 7minute spectrum belonging to phase A was included in phase B. Single spectra and chemical structure of SA (light blue) and DAD (green) are shown in (**B**).*

It begins with laccase-mediated removal of a hydrogen (one H^+ and one e^-) from the phenolic group of SA, leading to the formation of the corresponding phenoxy radical. In the following non-enzymatic step, two phenoxy radicals dimerize following the β-β coupling model.

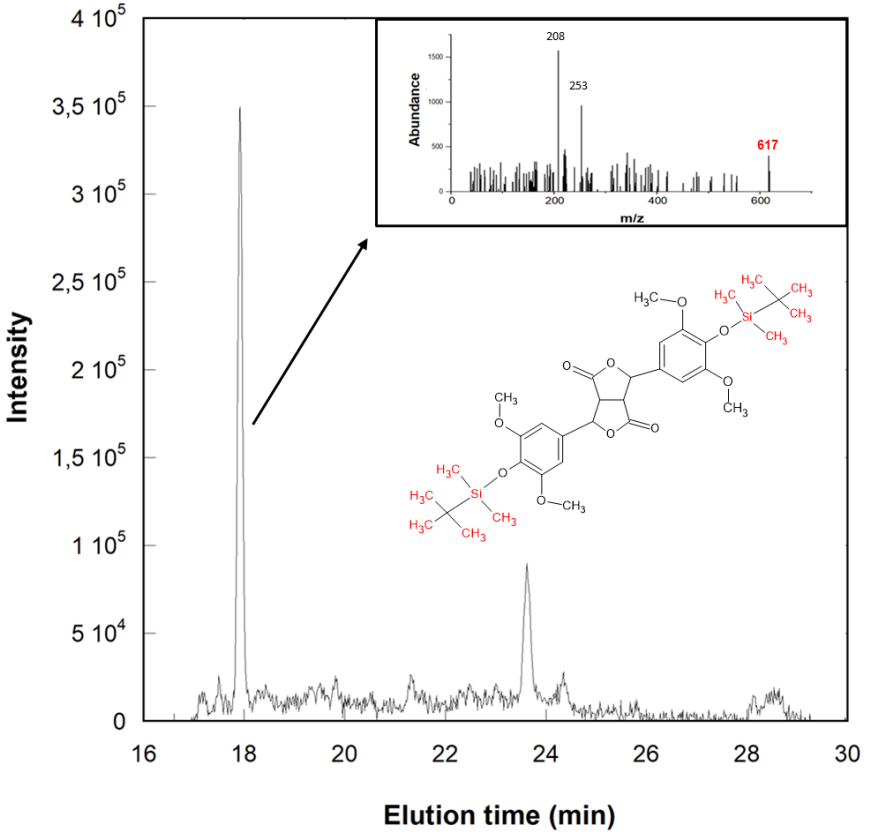

Figure 4.11 *Gas chromatography-mass spectrometry characterization DAD. Here is shown the GC-MS chromatogram of PcLAC reaction on sinapic acid stopped at the end of Phase A (moment of accumulation of DAD). The chromatogram shows a peak with a retention time of 17.8 min whose electron ionization (EI) mass spectra (insert) is compatible with DAD. The fragmentation pattern shows the presence of a characteristic ion (m/z 617) which can be the result of DAD derivatized with TBDMS. The chemical structure of DAD with the TBDMS derivatization is shown in red.*

In all studies conducted on laccase-mediated SA oxidation[67,68,70,71], the presence of dimers due to β-β coupling of radicals formed by laccase was observed. Of the possible SA dimers, the most represented is DAD, which was suggested to be the most thermodynamically stable form[40]. In this case, two DAD isomers are not distinguishable by UV/Vis spectroscopy due to overlapping spectra, apart from a slight shift of the absorption maximum from 208 to 204 nm[67].
To confirm the nature of the intermediate of Phase A as DAD, a -MS analysis was performed. The GS-mass spectra confirmed the presence in solution of a molecule whose MW was compatible with the presence of DAD as TBDMS (tert-butyldimethylsilyl chloride) derivative (***Figure 4.11***).

4.3.2 Oxidation of sinapic acid in presence of PcODH

Piumi et al. reported the ability of *Pc*ODH to slow down or inhibit laccase-mediated reactions on sinapic acid, coumaric acid, 2,6-dimethoxyphenol, and guaiacol[29]. These compounds were chosen to mimic some of the radical intermediates produced during lignin degradation, to understand the proposed role of *Pc*ODH in reducing phenoxy radicals and preventing their repolymerization.
Enzymatic reactions were performed in 50mM citrate phosphate buffer pH 4.5, 0.5mM sinapic acid, 1.5nkat/mL of laccase and 2.5 nkat/mL of ODH, as well as 500mM glucose as the ODH reducing substrate. The reaction was initiated by sequential addition of enzymes to the mixture and proceeded as observed with laccase only. However, the oxidation of sinapic acid, corresponding to decreasing absorbance at 233 and 315 nm, was slower for ODH/LAC than for laccase alone. As such, the end of phase A, when absorbance at 208 and 315 nm cease increasing and decreasing respectively, occurs at 12 min rather than at 7 min as observed for laccase alone. This finding suggests flavoenzyme-mediated reduction of the SA phenoxy radical, as it was hypothesized for PcODH[29] and related enzymes[30,50].

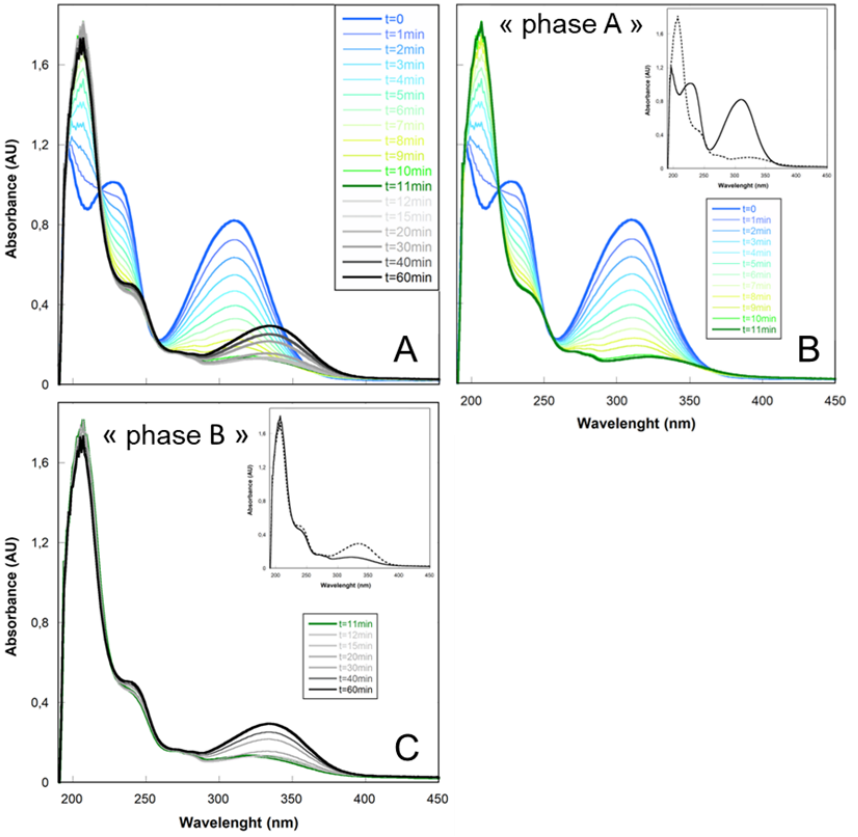

Figure 4.12 *Changes in the UV-Vis spectra of Rx4 of Table 4.1. The entire reaction (1h) is shown (**A**). Each line represents a different time of the reaction (see legends). The entire reaction has been devided in phase A (**A**) phase B (**B**). Inserts show the visible initial spectra (continuous line) and final spectra of phase A and phase B(dashed lies).*

Phase B of the laccase-mediated reaction is even more drastically affected by the presence of *Pc*ODH in solution, and no products that absorb between 450 nm and 550 nm are detected ***(Figure 4.12 C)***; in fact, the reaction mixture remains clear even after very long incubation of the reaction mixture. Laccase oxidation of DAD and accumulation of "reddish" products absorbing around 512nm without ODH, seems no to take place when the flavoenzyme is present. For the entire time

of the experiment (1h) the spectrum of DAD remains almost unaltered, except for a slight decrease of absorbance at 208 nm and an increase at 337nm (***Figure 4.12 C)***. This evolution of DAD's spectra was previously explained by Lacki et al.[67] as resulting from the thermolysis of DAD. In that study, nonenzymatic DAD thermolysis was noticeable at temperatures above 10°C and resulted in the formation of a product the Lacki and colleagues could not identify. To prove that the peak at 337nm is a signature of DAD thermolysis, *Pc*LAC reactions carried out at 30 and 10°C were stopped at the end of phase A (7min after the beginning of the reaction), using 1mM sodium azide to inhibit *Pc*LAC. It is possible to see that when the laccase reaction is performed and stopped at 30°C, the absorption peak at 337nm increases with time (***Figure 4.13 A)***, while at 10°C there is no detectable increase of absorption at 337nm (***Figure 4.13 B***).

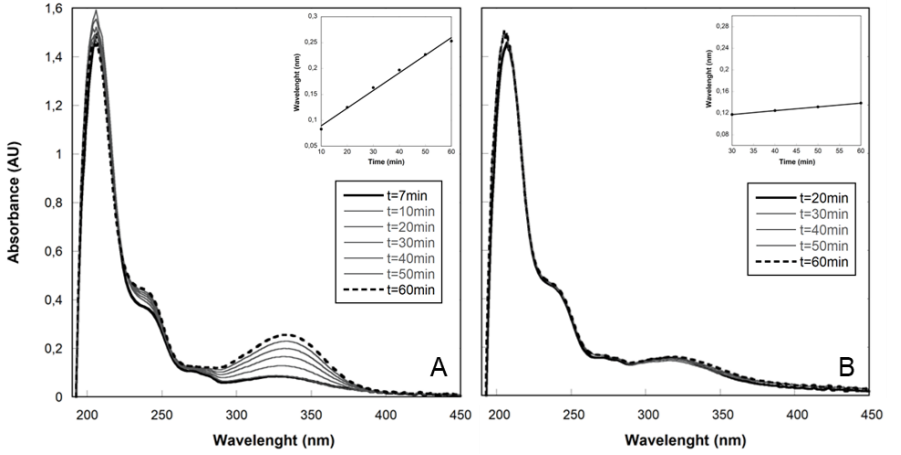

Figure 4.13 *Inhibition experiments of PcLAC with 1mM NaAzide performed at 30°C (**A**) and 10°C (**B**). Reaction times are shown in the legends. Inserts show the variation of absorbance at 337nm as a function of time.*

In both cases, after *Pc*LAC is deactivated, no transformation of DAD into red-shifted absorbing species is observed. This experiment provides us two information: i) the absorption peak at 337nm depends

on the DAD intrinsic instability at temperatures higher than 10°C and corresponds to a DAD thermolytic product; and ii) as Lacki et al demonstrated, phase B relies on DAD transformation by laccase, and is an alternative pathway to DAD thermolysis. Altogether these results show that in the presence of ODH, laccase-mediated oxidation of both SA and DAD seem to be slowed down, while DAD thermolysis become the prominent pathway, preventing further DAD oxidation by laccase.

To gain further insight into the synergistic actions of *Pc*ODH and *Pc*LAC, different ratios of these enzymes were tested in the same experimental conditions. The different ratios are shown in ***Table 4.3*** from Rx2 to Rx5. Rx1 and Rx4 correspond to the ratios used in the previously described experiments.

Table 4.3*: PcLAC and PcODH ratios used for all the experiments. All enzyme quantities are expressed in nkat/mL.*

	Rx1	**Rx2**	**Rx3**	**Rx4**	**Rx5**
PcLAC	1.5	1.5	1.5	1.5	1.5
PcODH	-	0.15	0.5	2.5	5.5

In the case of Rx2 and Rx3 the quantity of ODH is not enough and the reaction of laccase can proceed beyond DAD accumulation of phase A (***Figure 4.14 A)***, to phase B, accompanied by increased absorbance between 450 and 550 nm, as in experiments with laccase alone (***Figure 4.14 B)***. For both enzyme ratios, the increase of the peak at 515 nm (phase B) starts 8 minutes after the beginning of the reaction, as with laccase alone. Unlike with previously described reactions, increase of the reddish response (phase B) is followed by phase C: decrease of absorbance at 515nm, blue shift of the peak towards 421 nm, and concomitant increase of the thermolysis product peak at 337 nm (***Figure 4.14 C)***. The reaction turns from dark red during the reddish response (phase B) to yellowish after the blue shift (phase C), and the

new spectrum is stable up to 1 hour after the beginning of the experiment. These data suggest that ODH might reduce other laccase-generated intermediates beyond SA and DAD.

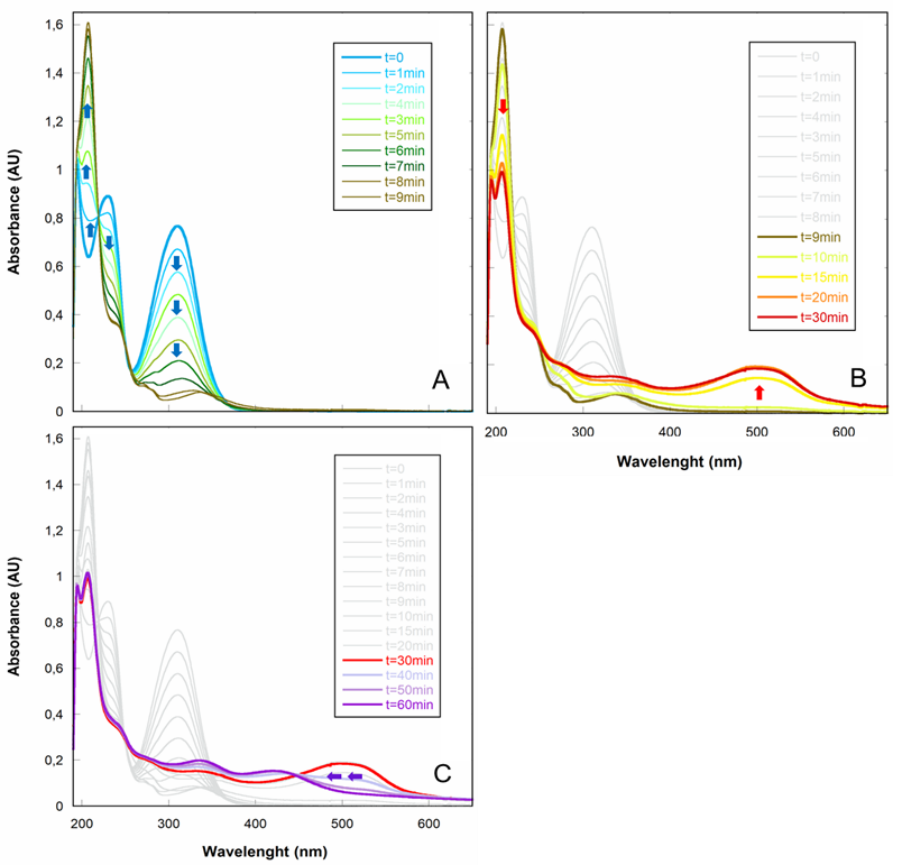

Figure 4.14 *Changes in the UV-Vis spectra of Rx2 of Table 4.1. The entire reaction has been devided in phase A of sinapic acid oxidation (A) phase B (B) and phase C (C) . Reaction times are shown in the legends***.**

The absorbance at 515 nm (considered for simplicity as the reference for the wide 450-550 nm peak), detected 25min after the reaction starts

(phase B), is shown for all enzyme ratios in ***Figure 4.15 A***. It is possible to see that up to Rx3, the reddish response (phase B) is inversely dependent on the concentration of ODH present in solution, while for the Rx4 ratio and higher ODH contents no reddish response is detected. On the contrary, for Rx4 and higher ODH contents, the peak at 337nm, recorded after 1 hour incubation at 30°C, is not dependent on *Pc*ODH concentration (***Figure 4.15 B)***, confirming a hypothetical DAD thermolysis product nonenzymatically generated.
To confirm that the observed phenomena were due to *Pc*ODH, control experiments were performed in the absence of the enzyme but with glucose in solution (data not shown). Tests performed in the absence of glucose (*Pc*ODH in the oxidized state) confirmed the ability of *Pc*ODH to reduce the radicals produced by laccase only in the reduced state (data not shown).

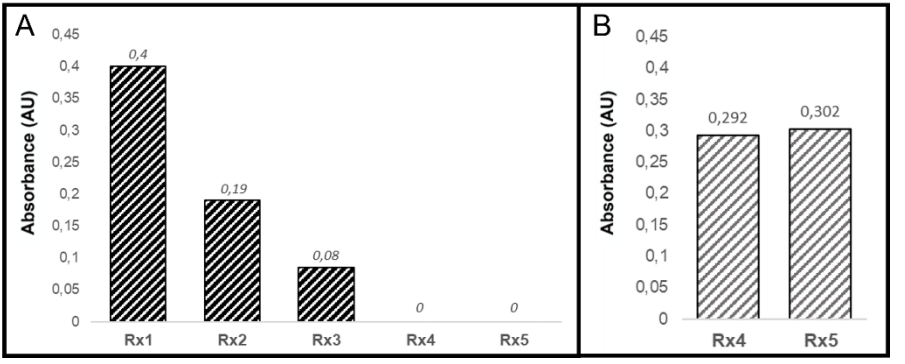

Figure 4.15 *Histograms of absorbance at 515nm of the different reactions of Table 4.1 registered at 25min after the start of the reactions (**A**) and absorbance at 337nm after 1h of the reaction Rx4 and Rx5 (**B**).*

4.4 Effect of *Pc*ODH on guaiacol oxidation by *Pc*LAC

Starting from the experiment of Piumi et al.[29], spectroscopic analysis has been performed to assess the ability of *Pc*ODH to revert *Pc*LAC-mediated guaiacol oxidation.
Reactions were performed in 50mM citrate phosphate pH 4.5 buffer, 0.5mM guaiacol at 30°C for 30minutes. *Pc*LAC and *Pc*ODH concentrations were chosen to be 5.6nkat/mL and 2.5nka/mLt respectively, reproducing the experiment of Piumi et al[29]. The reactions were monitored in 1 min acquisition steps between 190nm and 1200nm.
Changes in the UV absorbance spectrum of the reaction products, oxidized by *Pc*LAC, are shown in ***Figure 4.16 A***. Compared to reduced GA, two peaks at 412 and 470 nm start to appear quite early (5 min) after starting the reaction, and their heights increase up to plateau. These results are in accordance with what previously observed for the oxidation of guaiacol[72,73]. These products are mainly dimers produced by C–C radical coupling of two GA monomers oxidized by the enzyme and trimers that are the result of the same mechanism on dimers of GA. All these products absorb in the range of 350nm and 550nm[72].
When *Pc*ODH is present in the reaction mixture, no increase in absorbance at the peaks 412nm and 470nm is detected (***Figure 4.16 B***).
The spectra of guaiacol are stable and superposable to the initial spectrum throughout all the observation (30 min). These data suggest that *Pc*ODH can successfully prevent the accumulation of any laccase-generated guaiacol oxidation product. As described preciously[29,50], the inhibition capacity (intended as the ability of *Pc*ODH to reduce the radicals produced by PcLAC and therefore inhibit accumulation of the reaction products) is complete, in these experimental conditions.

Figure 4.16 *Changes in the UV-Vis spectra of guaiacol during oxidation by PcLAC in absence (**A**) and in presence of PcODH (**B**). Reaction times are shown in the legends. Inserts show the visible initial spectra (continuous line) and after 30min (dashed lies).*

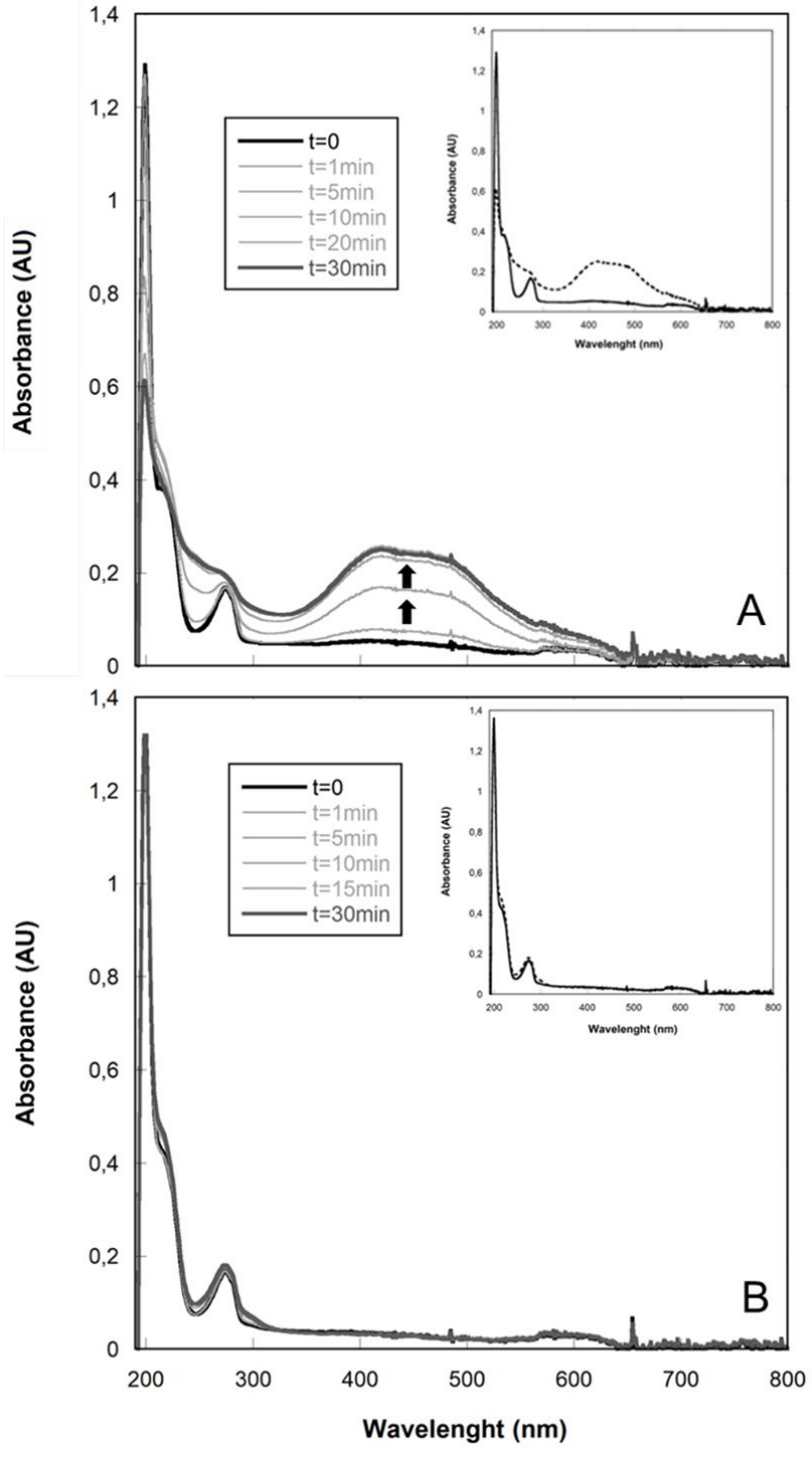
Absorbance (AU)
1,4
1,2
1
0,8
0,6
0,4
0,2
0
t=0
t=1min
t=5min
t=10min
t=20min
t=30min
Absorbance (AU)
Wavelenght (nm)
A
t=0
t=1min
t=5min
t=10min
t=15min
t=30min
B
200
300
400
500
600
700
800
Wavelenght (nm)

Discussion

The biological mechanism of lignin degradation involves the orchestration of numerous enzymes. Among them, laccases participate to the earliest steps of lignin degradation by oxidative attack of phenolic substrates and concomitant generation of phenoxy radicals. These highly reactive radicals species can however spontaneously rearrange themselves and cross-react, resulting in high molecular weight species, and hence causing repolymerization *in vitro*[49,70]. The hypothesis that AA3_2 enzymes might prevent the accumulation of oxidation products resulting from the radical coupling of substrates oxidized by laccase is not new[29,30,49,50]. However, this is the first time that detailed functional data and, most importantly, structural evidence are provided that validate the hypothesis and help elucidating laccase-driven mechanisms.

The three structures reported herein provide the first structural evidence for the ability of *Pc*ODH to bind aromatics, such as sinapic acid and guaiacol, analogues of molecules and phenoxy radicals derived from the oxidative breakdown of lignin. These data confirm what has been observed in *Pc*ODH structures bound to electron donors, notably: (i) the lack of binding specificity of residues facing the active site; (ii) the presence of three aromatic residues involved in substrate stabilization and orientation, Phe421, Phe416 and Tyr64; (iii) the involvement of a substrate biding loop; and (iv) the binding specificity of SBS for carbohydrate substrates[51]. Structural analysis suggests that hydrogen bonds do not play a major role in electron acceptor recognition, as it was observed for glucose and laminaribiose binding, and that the molecular determinants of enzyme-ligand complex formation rely on platforms of aromatic amino acids (Phe421, Phe416 and Tyr64). These residues, together with Trp430, can establish CH-π interactions with oxidizable saccharide substrates and π–π stacking with the aromatic rings of electron acceptors analogues such as synapic acid and guaiacol. Indeed, all three structures in complex with electron acceptors analogues, the ligands closer to the FAD cofactor were positioned between Phe416 and Tyr64

and slightly further away from Trp430, reminiscent of the position of the glucose alpha anomer. When a second SA was present in the active site, it interacted with Phe421. This residue is part of a substrate binding loop that adopts a close conformation upon binding of two glucose molecules or laminaribiose. Although in *Pc*ODH-SA*t* the closed conformation of the substrate binding loop is due to crystal packing, binding of synapic acid at this site is reminiscent of saccharide binding in *Pc*ODH structures in complex with glucose or laminaribiose. Further on, in *Pc*ODH-SA*o* and *Pc*ODH-GA structures, in which the substrate binding loop is exposed to the solvent in an open conformation, Phe421 interacts with sinapic acid and guaiacol, also stabilized by stacking with His346. Given the mobility and flexibility of the binding loop, a shattering mechanism could be imagined in which Phe421 accompanies the two ligands inside the active site. This hypothesis is also supported by the tendency of both electron donors and acceptors to localize, in the crystallographic structures, along what seems to be a ligand diffusion path, that runs from the solvent-exposed active site funnel to the buried FAD cofactor.

The position of guaiacol in ODH active site is worth noting: it interacts with Phe416 and Ty64, like the aromatic moiety of sinapic acid, but not with catalytic His528, His571 and FAD, not possessing the long carboxylic tail found in SA. As such, stuck between the two aromatic residues Phe416 and Tyr64, GA is too far away from the cofactor and the catalytic histidines to comply with a hydride transfer mechanism, as proposed for GDH[66] and GOX[43] enzymes. In the event of a radical enzymatic mechanism, our data might also suggest an unexpected role for Try64, which, in addition to acting as a support for ligand stabilization, might be involved in electron transfer during the reaction with phenoxy radicals. In fact, this tyrosine is conserved in other AA3_2 oxidoreductases, such as *Af*GDH (Ty53)[66] and *An*GOX (Tyr68)[43], and tyrosine is usually involved in electron transfer chains, which include FAD cofactors[74]. Moreover, the distance of Tyr64 to guaiacol and FAD (3.9 and 4.9 Å respectively) is compatible with electron transfer[74,75]. Previous functional and structural analysis confirmed *Pc*ODH ability to bind oligosaccharides (like laminaribiose). In ODH active site, both saccharide-binding sites that

cooperatively bind laminaribiose are also able to interact independently with monosaccharides. The same is probably true with aromatic electron acceptors, as revealed by the structure of *Pc*ODH-SA*t*, in which the positions of two SA ligands are reminiscent of those occupied by laminaribiose glycosyl units. The hypothesis that the crystallographic structures presented here are representative of ODH binding to electron acceptor analogues is also supported by functional data. In fact, when *Pc*ODH is present, the reaction profiles of laccase-mediated oxidation of SA and GA changes profoundly. As observed by Lacki et al.[67], SA oxidation by PcLAC was found to be divided into two phases, A and B (***Figure 5.1 A***), in which the DAD intermediate is formed at the end of phase A, then further oxidized to enter phase B. As considered by the authors, the presence of two distinct phases could be due to the difference in the optimum pH for the enzymatic transformations of SA and DAD. The phase A of laccase-mediated oxidation of SA (***Figure 4.12, Figure 5.1***), which corresponds to the moment of accumulation of dehydrodisinapic acid (DAD), is slowed down by PcODH. Moreover, instead of proceeding to phase B, which would involve laccase-mediated oxidation of DAD, an equilibrium towards the reduced DAD form is established, do to ODH activity (***Figure 5.1 B***). This equilibrium provides the necessary time necessary for DAD to undergo thermolysis. Finally, thermolyzed DAD is not subject to further laccase-mediated oxidation, so the pull of generated reactive radical species does not grow bigger and repolymerization cannot occur. A possible mechanism explaining *Pc*ODH action during *Pc*LAC oxidation of sinapic acid is shown in ***Figure 5.1 B***: the promiscuity of ODH active site allows it to be active on both SA radicals (slowing down phase A) and DAD radicals (avoiding the trigger of phase B). Our functional data suggest that *Pc*ODH can bind DAD and similar molecules. In fact, superimposition of the chemical structure of DAD on the two SAs bound to *Pc*ODH-SA*t*, confirm possible DAD binding to ODH active site (***Figure 5.2***).

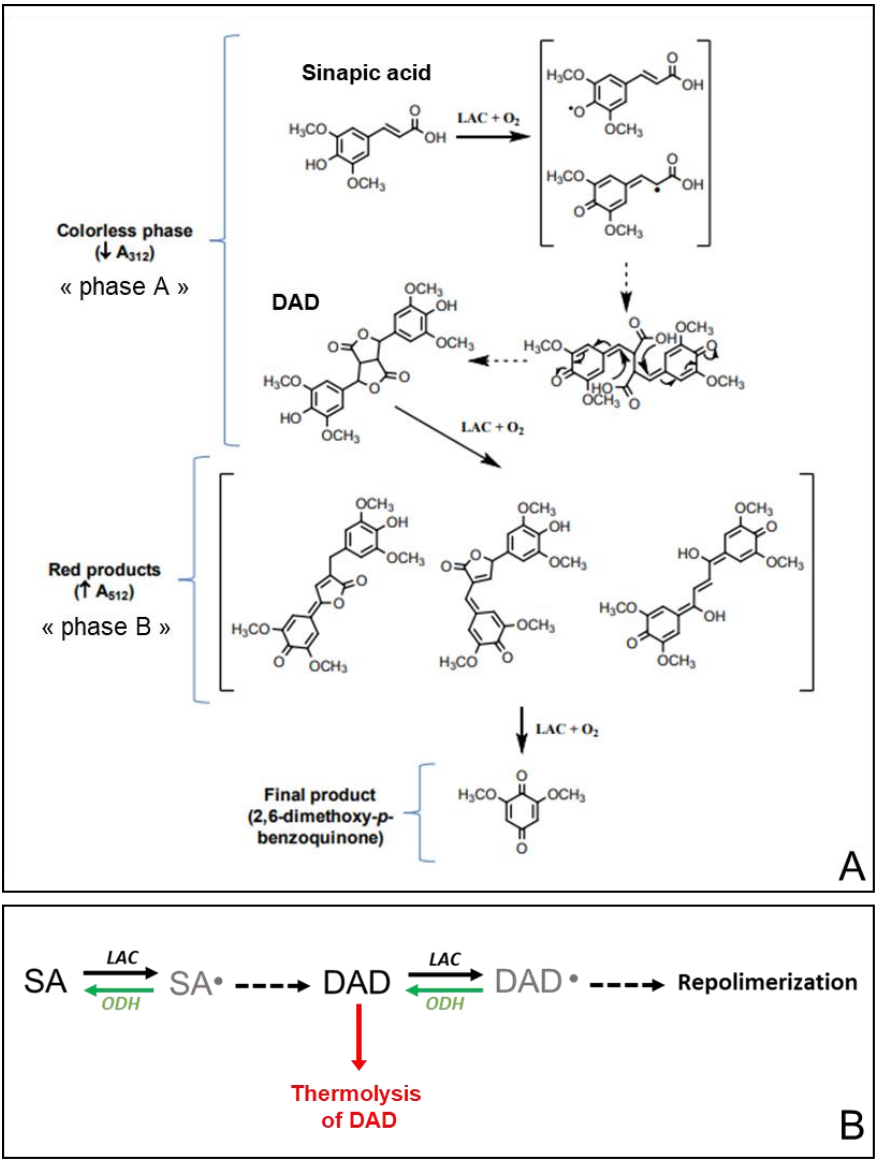

Figure 5.1 *Reaction pathway for SA oxidation by Laccase from Parco et al.*[68]*. The main oxidation intermediates proposed by Lacki et al.*[67] *are represented. Solid arrows indicate reaction steps catalyzed by laccase. Dashed arrows indicate non-enzymatic steps (**A**). Scheme of mechanism of action hypothesis for PcODH during SA oxidation by PcLAC (**B**).*

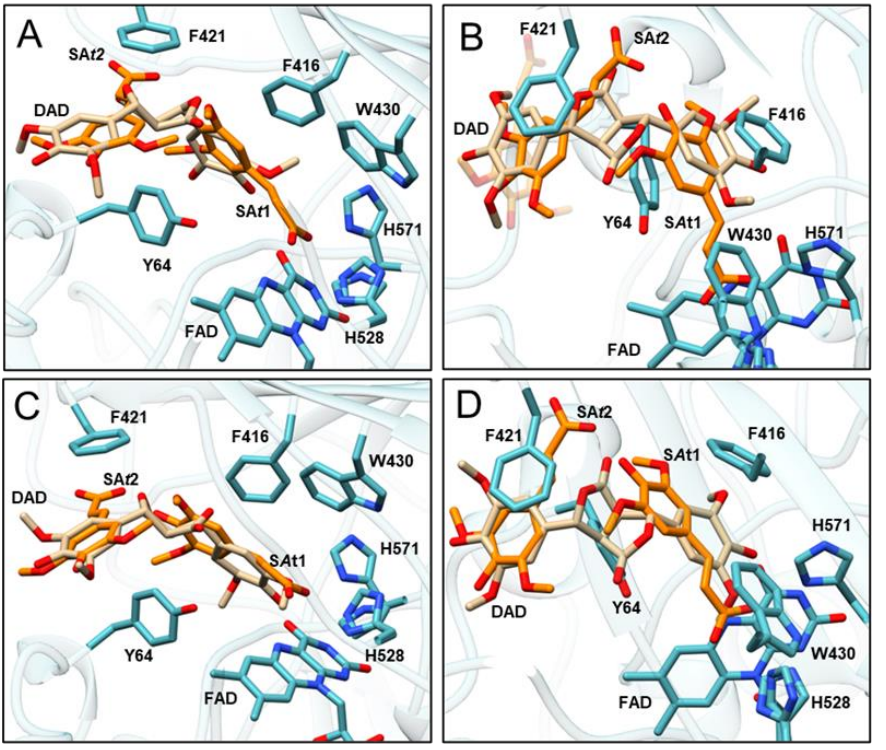

Figure 5.2 *Hypotheses on the location of DAD within the active site of PcODH. Sinapic acids SAt1 and SAt2 are represented by orange sticks, whereas DAD is represented by yellow sticks. The 3D structure of DAD was obtained from PubcChem site (https://pubchem.ncbi.nlm.nih.gov/compound/11155045#section=3D-Conformer), The sdf file has been converted to a pdb file through eLBOW (Phenix suite). Panels* ***A*** *and* ***B*** *represent the superposition of DAD on SAt1 and SAt2 (PcODH-SAt structure), giving priority to the aromatic rings positions. Panels* ***C*** *and* ***D*** *represent the position of DAD hypothesized if it was aligned to Phe416 and Phe421. Without the constraint given by the tail of the synaptic acid (SAt1), DAD would have been positioned closer to the FAD cofactor.*

Conclusion and future perspectives

Structural and functional characterization of *Pc*ODH, described in this thesis, provides unexpected insights into its role as an auxiliary enzyme, supporting laccase during the lignin degradation process.
Structural analysis of *Pc*ODH in complex with sinapic acid and guaiacol provided details on its recognition mechanism with electron acceptor analogues: the enzyme promiscuity and the major role of aromatic rings in stabilizing and orienting different substrates and co-substrates in the active site were confirmed.
Functional studies performed on *Pc*ODH and PcLAC allowed us to further investigate the synergistic action of these two enzymes *in vitro*: when *Pc*ODH is in the reduced state, it can reduce phenoxy radicals produced by laccase oxidation and avoid the accumulation and repolymerization of oxidative products. Moreover, the structure in complex with two sinapic acids in the active site points to possible *Pc*ODH binding to dimers (*i.e* DAD) that derive from coupling of monomeric phenoxy radicals.
Position of GA in the crystallographic structures suggests that a radical mechanism should maybe be considered, as an alternative to the hydride transfer mechanism proposed for the electron donors. The latter in fact requires substrate binding to His528 and His571, which is impossible for GA. If a radical mechanism is to be considered, a new role for Tyr64 has to be hypothesized too. To understand the role of this tyrosine, further experiments, including site-directed mutagenesis, need to be performed. One possibility would be to mutate Tyr64 in phenylalanine to compromise the electron transfer reaction of the supposed radical mechanism while maintaining aromatic stacking with the ligands.
The work presented in this thesis further exemplifies *Pc*ODH promiscuity and its ability to bind diverse substrate molecules. Indeed, as already seen for glucose and laminaribiose bound to *Pc*ODH[51], two sinapic molecules in ODH active site, as observed in *Pc*ODH-SA*t*, support the hypothesis of possible binding with DAD. Therefore, crystal structure of the ODH-DAD complex is necessary to confirm

the involvement of such an intermediate. Achieving this goal would require to establish a production protocol to isolate and extract DAD for soaking experiments.

With the aim of further investigating the relationship between *Pc*ODH and *Pc*LAC, it would be interesting to repeat the experiments at different ratios of ODH and LAC but at limiting glucose concentrations, rather than at 500 mM as performed in this work.

To gain deeper insight into *Pc*ODH reaction mechanism with phenoxy radicals, and into possible FAD radical species, EPR experiments could be performed, as in was done for Veratryl Alcohol Oxidase from *Pleurotus ostreatus*[49].

Finally, to further explore the properties and physiological role of ODH within the context of lignocellulose breakdown, functional and structural studies should be extended to other laccase model substrates, as well as to analogues of lignin degradation products. During the implementation of this PhD project, three more *Pc*ODH structures in complex with electron acceptors analogues were solved, confirming the soundness of our hypothesis, although they have not been shown for the sake of clarity. Functional studies probing these molecules as *Pc*LAC substrates and *Pc*ODH electron acceptors will possibly unveil novel details of the complex synergy between these two enzymatic activities.

A more detailed understanding of the mechanisms of action of auxiliary activity enzymes involved in lignocellulose degradation is still a research priority.

Bibliography

(1) Cosgrove, D. J. Growth of the Plant Cell Wall. *Nat. Rev. Mol. Cell Biol.* **2005**, *6* (11), 850–861. https://doi.org/10.1038/nrm1746.

(2) Keegstra, K. Plant Cell Walls. *Plant Physiol.* **2010**, *154* (2), 483–486. https://doi.org/10.1104/pp.110.161240.

(3) Somerville, C. Cellulose Synthesis in Higher Plants. **2006**. https://doi.org/10.1146/annurev.cellbio.22.022206.160206.

(4) Payne, C. M.; Knott, B. C.; Mayes, H. B.; Hansson, H.; Himmel, M. E.; Sandgren, M.; Ståhlberg, J.; Beckham, G. T. Fungal Cellulases. *Chem. Rev.* **2015**, *115* (3), 1308–1448. https://doi.org/10.1021/cr500351c.

(5) Ruiz-duen, F. J. Substrate Oxidation Sites in Versatile Peroxidase and Other Basidiomycete Peroxidases. **2009**, *60* (2), 441–452. https://doi.org/10.1093/jxb/ern261.

(6) Cragg, S. M.; Beckham, G. T.; Bruce, N. C.; Bugg, T. D. H.; Distel, D. L.; Dupree, P.; Etxabe, A. G.; Goodell, B. S.; Jellison, J.; McGeehan, J. E.; McQueen-Mason, S. J.; Schnorr, K.; Walton, P. H.; Watts, J. E. M.; Zimmer, M. Lignocellulose Degradation Mechanisms across the Tree of Life. *Curr. Opin. Chem. Biol.* **2015**, *29*, 108–119. https://doi.org/10.1016/j.cbpa.2015.10.018.

(7) Kracher, D.; Scheiblbrandner, S.; Felice, A. K. G.; Breslmayr, E.; Preims, M.; Ludwicka, K.; Haltrich, D.; Eijsink, V. G. H.; Ludwig, R. Extracellular Electron Transfer Systems Fuel Cellulose Oxidative Degradation. *Science (80-.).* **2016**, *352* (6289), 1098–1101. https://doi.org/10.1126/science.aaf3165.

(8) Janusz, G.; Pawlik, A.; Sulej, J.; Świderska-Burek, U.; Jarosz-Wilkolazka, A.; Paszczyński, A. Lignin Degradation: Microorganisms, Enzymes Involved, Genomes Analysis and Evolution. *FEMS Microbiol. Rev.* **2017**, *41* (6), 941–962. https://doi.org/10.1093/femsre/fux049.

(9) Cantarel, B. L.; Coutinho, P. M.; Rancurel, C.; Bernard, T.; Lombard, V.; Henrissat, B. The Carbohydrate-Active EnZymes Database (CAZy): An Expert Resource for

Glycogenomics. **2009**, *37* (October 2008), 233–238. https://doi.org/10.1093/nar/gkn663.
(10) Levasseur, A.; Drula, E.; Lombard, V.; Coutinho, P. M.; Henrissat, B. Expansion of the Enzymatic Repertoire of the CAZy Database to Integrate Auxiliary Redox Enzymes. *Biotechnol. Biofuels* **2013**, *6* (1), 1–14. https://doi.org/10.1186/1754-6834-6-41.
(11) Sützl, L.; Laurent, C. V. F. P.; Abrera, A. T.; Schütz, G.; Ludwig, R.; Haltrich, D. Multiplicity of Enzymatic Functions in the CAZy AA3 Family. *Appl. Microbiol. Biotechnol.* **2018**, *102* (6), 2477–2492. https://doi.org/10.1007/s00253-018-8784-0.
(12) Cao, L.; Yu, I. K. M.; Liu, Y.; Ruan, X.; Tsang, D. C. W.; Hunt, A. J.; Ok, Y. S.; Song, H.; Zhang, S. Lignin Valorization for the Production of Renewable Chemicals: State-of-the-Art Review and Future Prospects. *Bioresour. Technol.* **2018**, *269* (August), 465–475. https://doi.org/10.1016/j.biortech.2018.08.065.
(13) Pollegioni, L.; Tonin, F.; Rosini, E. Lignin-Degrading Enzymes. *FEBS J.* **2015**, *282* (7), 1190–1213. https://doi.org/10.1111/febs.13224.
(14) Ros Barceló, A.; Gómez Ros, L. V.; Gabaldón, C.; López-Serrano, M.; Pomar, F.; Carrión, J. S.; Pedreño, M. A. Basic Peroxidases: The Gateway for Lignin Evolution? *Phytochem. Rev.* **2004**, *3* (1–2), 61–78. https://doi.org/10.1023/B:PHYT.0000047803.49815.1a.
(15) Glaeser, J. A. Mycological Society of America. *IMA Fungus* **2011**, *2* (2), 49–50. https://doi.org/10.1080/00275514.1942.12020904.
(16) Liers, C.; Arnstadt, T.; Ullrich, R.; Hofrichter, M. Patterns of Lignin Degradation and Oxidative Enzyme Secretion by Different Wood- and Litter-Colonizing Basidiomycetes and Ascomycetes Grown on Beech-Wood. *FEMS Microbiol. Ecol.* **2011**, *78* (1), 91–102. https://doi.org/10.1111/j.1574-6941.2011.01144.x.
(17) Hatti-kaul, R.; Ibrahim, V. Lignin-Degrading Enzymes: An Overview. **2013**, 167–192.

(18) Kirk, T. K.; Gifford, O.; Drive, P.; Farrell, R. L. ENZIMATIC " COMBUSTION ": THE MICROBIAL DEGRADATION OF. **1987**, 465–505.
(19) Wong, D. W. S. *Structure and Action Mechanism of Ligninolytic Enzymes*; 2009; Vol. 157. https://doi.org/10.1007/s12010-008-8279-z.
(20) Hammel, K. E.; Cullen, D. Role of Fungal Peroxidases in Biological Ligninolysis. *Curr. Opin. Plant Biol.* **2008**, *11* (3), 349–355. https://doi.org/10.1016/j.pbi.2008.02.003.
(21) Conesa, A.; Punt, P. J.; Van Den Hondel, C. A. M. J. J. Fungal Peroxidases: Molecular Aspects and Applications. *J. Biotechnol.* **2002**, *93* (2), 143–158. https://doi.org/10.1016/S0168-1656(01)00394-7.
(22) Levasseur, A.; Lomascolo, A.; Chabrol, O.; Ruiz-Dueñas, F. J.; Boukhris-Uzan, E.; Piumi, F.; Kües, U.; Ram, A. F. J.; Murat, C.; Haon, M.; Benoit, I.; Arfi, Y.; Chevret, D.; Drula, E.; Kwon, M. J.; Gouret, P.; Lesage-Meessen, L.; Lombard, V.; Mariette, J.; Noirot, C.; Park, J.; Patyshakuliyeva, A.; Sigoillot, J. C.; Wiebenga, A.; Wösten, H. A. B.; Martin, F.; Coutinho, P. M.; de Vries, R. P.; Martínez, A. T.; Klopp, C.; Pontarotti, P.; Henrissat, B.; Record, E. The Genome of the White-Rot Fungus Pycnoporus Cinnabarinus: A Basidiomycete Model with a Versatile Arsenal for Lignocellulosic Biomass Breakdown. *BMC Genomics* **2014**, *15* (1), 1–24. https://doi.org/10.1186/1471-2164-15-486.
(23) Giardina, P.; Faraco, V. Laccases: A Never-Ending Story. **2010**, 369–385. https://doi.org/10.1007/s00018-009-0169-1.
(24) Solomon, E. I.; Penfield, K. W.; Gewirth, A. A.; Lowery, M. D.; Shadle, S. E.; Guckert, J. A.; Lacroix, L. B. D SSlg and Geometry. **1996**, *243*, 67–78.
(25) Shraddha; Shekher, R.; Sehgal, S.; Kamthania, M.; Kumar, A. Laccase: Microbial Sources, Production, Purification, and Potential Biotechnological Applications. *Enzyme Res.* **2011**, *2011* (1). https://doi.org/10.4061/2011/217861.
(26) Kawai, S.; Nakagawa, M.; Ohashi, H. Degradation Mechanisms of a Nonphenolic β-O-4 Lignin Model Dimer by *Trametes Versicolor* Laccase in the Presence of 1-

Hydroxybenzotriazole. *Enzyme Microb. Technol.* **2002**, *30* (4), 482–489. https://doi.org/10.1016/S0141-0229(01)00523-3.
(27) Kawai, S.; Asukai, M.; Ohya, N.; Okita, K.; Ito, T.; Ohashi, H. Degradation of a Non-Phenolic β-O-4 Substructure and of Polymeric Lignin Model Compounds by Laccase of *Coriolus Versicolor* in the Presence of 1-Hydroxybenzotriazole. *FEMS Microbiol. Lett.* **1999**, *170* (1), 51–57. https://doi.org/10.1016/S0378-1097(98)00523-0.
(28) Camarero, S.; Cañas, A. I.; Nousiainen, P.; Record, E.; Lomascolo, A.; Martínez, M. J.; Martínez, Á. T. P-Hydroxycinnamic Acids As Natural Mediators for Laccase Oxidation of Recalcitrant Compounds. *Environ. Sci. Technol.* **2008**, *42* (17), 6703–6709. https://doi.org/10.1021/es8008979.
(29) Piumi, F.; Levasseur, A.; Navarro, D.; Zhou, S.; Mathieu, Y.; Ropartz, D.; Ludwig, R.; Faulds, C. B.; Record, E. A Novel Glucose Dehydrogenase from the White-Rot Fungus *Pycnoporus Cinnabarinus*: Production in *Aspergillus Niger* and Physicochemical Characterization of the Recombinant Enzyme. *Appl. Microbiol. Biotechnol.* **2014**, *98* (24), 10105–10118. https://doi.org/10.1007/s00253-014-5891-4.
(30) Mathieu, Y.; Piumi, F.; Valli, R.; Aramburu, J. C.; Ferreira, P.; Faulds, C. B.; Record, E. Activities of Secreted Aryl Alcohol Quinone Oxidoreductases from *Pycnoporus Cinnabarinus* Provide Insights into Fungal Degradation of Plant Biomass. *Appl. Environ. Microbiol.* **2016**, *82* (8), 2411–2423. https://doi.org/10.1128/AEM.03761-15.
(31) Couturier, M.; Mathieu, Y.; Li, A.; Navarro, D.; Drula, E.; Haon, M.; Grisel, S.; Ludwig, R.; Berrin, J. G. Characterization of a New Aryl-Alcohol Oxidase Secreted by the Phytopathogenic Fungus *Ustilago Maydis*. *Appl. Microbiol. Biotechnol.* **2016**, *100* (2), 697–706. https://doi.org/10.1007/s00253-015-7021-3.
(32) Daou, M.; Yassine, B.; Wikee, S.; Record, E.; Duprat, F.; Bertrand, E.; Faulds, C. B. *Pycnoporus Cinnabarinus* Glyoxal Oxidases Display Differential Catalytic Efficiencies on 5-Hydroxymethylfurfural and Its Oxidized Derivatives. *Fungal Biol. Biotechnol.* **2019**, *6* (1), 1–15.

https://doi.org/10.1186/s40694-019-0067-8.
(33) Daou, M.; Faulds, C. B. Glyoxal Oxidases: Their Nature and Properties. *World J. Microbiol. Biotechnol.* **2017**, *33* (5), 0. https://doi.org/10.1007/s11274-017-2254-1.
(34) Daou, M.; Piumi, F.; Cullen, D.; Record, E.; Faulds, C. B. Heterologous Production and Characterization of Two Glyoxal Oxidases from *Pycnoporus Cinnabarinus*. *Appl. Environ. Microbiol.* **2016**, *82* (16), 4867–4875. https://doi.org/10.1128/AEM.00304-16.
(35) Miyauchi, S.; Navarro, D.; Grisel, S.; Chevret, D.; Berrin, J. G.; Rosso, M. N. The Integrative Omics of White-Rot Fungus Pycnoporus Coccineus Reveals Co-Regulated CAZymes for Orchestrated Lignocellulose Breakdown. *PLoS One* **2017**, *12* (4), 1–17. https://doi.org/10.1371/journal.pone.0175528.
(36) Miyauchi, S.; Hage, H.; Drula, E.; Lesage-Meessen, L.; Berrin, J. G.; Navarro, D.; Favel, A.; Chaduli, D.; Grisel, S.; Haon, M.; Piumi, F.; Levasseur, A.; Lomascolo, A.; Ahrendt, S.; Barry, K.; LaButti, K. M.; Chevret, D.; Daum, C.; Mariette, J.; Klopp, C.; Cullen, D.; de Vries, R. P.; Gathman, A. C.; Hainaut, M.; Henrissat, B.; Hildén, K. S.; Kües, U.; Lilly, W.; Lipzen, A.; Mäkelä, M. R.; Martinez, A. T.; Morel-Rouhier, M.; Morin, E.; Pangilinan, J.; Ram, A. F. J.; Wösten, H. A. B.; Ruiz-Dueñas, F. J.; Riley, R.; Record, E.; Grigoriev, I. V.; Rosso, M. N. Conservedwhite-Rot Enzymaticmechanismfor Wood Decay in the Basidiomycota Genus *Pycnoporus*. *DNA Res.* **2020**, *27* (2), 1–14. https://doi.org/10.1093/DNARES/DSAA011.
(37) Wongnate, T.; Chaiyen, P. The Substrate Oxidation Mechanism of Pyranose 2-Oxidase and Other Related Enzymes in the Glucose-Methanol-Choline Superfamily. *FEBS J.* **2013**, *280* (13), 3009–3027. https://doi.org/10.1111/febs.12280.
(38) Oxidases, F.; Gadda, G. Hydride Transfer Made Easy in the Reaction of Alcohol Oxidation Catalyzed By. **2008**, 13745–13753.
(39) Hallberg, B. M.; Henriksson, G.; Vasella, A.; Divne, C.; Zu, C.-. Mechanism of the Reductive Half-Reaction in Cellobiose

Dehydrogenase *. **2003**, *278* (9), 7160–7166. https://doi.org/10.1074/jbc.M210961200.
(40) Quaye, O.; Lountos, G. T.; Fan, F.; Orville, A. M.; Gadda, G.; August, R. V; Re, V.; Recei, M.; No, V. Role of Glu312 in Binding and Positioning of the Substrate for the Hydride Transfer Reaction in Choline Oxidase †,‡. **2008**, 243–256.
(41) Hallberg, B. M.; Leitner, C.; Haltrich, D.; Divne, C. Crystal Structure of the 270 KDa Homotetrameric Lignin-Degrading Enzyme Pyranose 2-Oxidase. **2004**, 781–796. https://doi.org/10.1016/j.jmb.2004.06.033.
(42) Tan, T. C.; Spadiut, O.; Wongnate, T.; Sucharitakul, J.; Krondorfer, I.; Sygmund, C.; Haltrich, D.; Chaiyen, P.; Peterbauer, C. K.; Divne, C. ˚ Crystal Structure of Pyranose Dehydrogenase from Agaricus Meleagris Rationalizes Substrate Specificity and Reveals a Flavin Intermediate. **2013**, *8* (1). https://doi.org/10.1371/journal.pone.0053567.
(43) Hecht, H. J.; Kalisz, H. M.; Hendle, J.; Schmid, R. D.; Schomburg, D. Crystal Structure of Glucose Oxidase from *Aspergillus Niger* Refined at 2.3 Å Reslution. *Journal of Molecular Biology*. 1993, pp 153–172. https://doi.org/10.1006/jmbi.1993.1015.
(44) Arevalo-Gallegos, A.; Ahmad, Z.; Asgher, M.; Parra-Saldivar, R.; Iqbal, H. M. N. Lignocellulose: A Sustainable Material to Produce Value-Added Products with a Zero Waste Approach—A Review. *Int. J. Biol. Macromol.* **2017**, *99*, 308–318. https://doi.org/10.1016/j.ijbiomac.2017.02.097.
(45) Cao, Y.; Chen, S. S.; Zhang, S.; Ok, Y. S.; Matsagar, B. M.; Wu, K. C. W.; Tsang, D. C. W. Advances in Lignin Valorization towards Bio-Based Chemicals and Fuels: Lignin Biorefinery. *Bioresour. Technol.* **2019**, *291* (May). https://doi.org/10.1016/j.biortech.2019.121878.
(46) Beckham, G. T.; Johnson, C. W.; Karp, E. M.; Salvachúa, D.; Vardon, D. R. Opportunities and Challenges in Biological Lignin Valorization. *Curr. Opin. Biotechnol.* **2016**, *42* (March), 40–53. https://doi.org/10.1016/j.copbio.2016.02.030.
(47) Levasseur, A.; Drula, E.; Lombard, V.; Coutinho, P. M.; Henrissat, B. Expansion of the Enzymatic Repertoire of the

CAZy Database to Integrate Auxiliary Redox Enzymes. *Biotechnol. Biofuels* **2013**, *6* (1), 1. https://doi.org/10.1186/1754-6834-6-41.
(48) Bugg, T. D. H.; Rahmanpour, R. Enzymatic Conversion of Lignin into Renewable Chemicals. *Curr. Opin. Chem. Biol.* **2015**, *29*, 10–17. https://doi.org/10.1016/j.cbpa.2015.06.009.
(49) Marzullo, L.; Cannio, R.; Giardina, P.; Santini, M. T.; Sannia, G. Veratryl Alcohol Oxidase from *Pleurotus Ostreatus* Participates in Lignin Biodegradation and Prevents Polymerization of Laccase-Oxidized Substrates. *J. Biol. Chem.* **1995**, *270* (8), 3823–3827. https://doi.org/10.1074/jbc.270.8.3823.
(50) Sygmund, C.; Klausberger, M.; Felice, A. K.; Ludwig, R. Reduction of Quinones and Phenoxy Radicals by Extracellular Glucose Dehydrogenase from *Glomerella Cingulata* Suggests a Role in Plant Pathogenicity. *Microbiology* **2011**, *157* (11), 3203–3212. https://doi.org/10.1099/mic.0.051904-0.
(51) Cerutti, G.; Gugole, E.; Montemiglio, L. C.; Turbé-Doan, A.; Chena, D.; Navarro, D.; Lomascolo, A.; Piumi, F.; Exertier, C.; Freda, I.; Vallone, B.; Record, E.; Savino, C.; Sciara, G. Crystal Structure and Functional Characterization of an Oligosaccharide Dehydrogenase from *Pycnoporus Cinnabarinus* Provides Insights into Fungal Breakdown of Lignocellulose. *Biotechnol. Biofuels* **2021**, *14* (1), 1–18. https://doi.org/10.1186/s13068-021-02003-y.
(52) Delattre, M.; Robert, J. L.; Georis, J.; Lomascolo, A.; Record, E.; Herpoe, I. Overproduction of Laccase by a Monokaryotic Strain of Pycnoporus Cinnabarinus Using Ethanol as Inducer. **2003**, 618–624.
(53) Kabsch, W. XDS. *Acta Crystallogr. Sect. D Biol. Crystallogr.* **2010**, *66* (2), 125–132. https://doi.org/10.1107/S0907444909047337.
(54) Vagin, A.; Teplyakov, A. A Translation-Function Approach for Heavy-Atom Location in Macromolecular Crystallography. *Acta Crystallogr. Sect. D Biol. Crystallogr.* **1998**, *54* (3), 400–402. https://doi.org/10.1107/S0907444997014923.

(55) Collaborative Computational Project, N. 4. The CCP4 Suite: Programs for Protein Crystallography. *Acta Crystallogr. Sect. D Biol. Crystallogr.* **1994**, *50* (5), 760–763. https://doi.org/10.1107/S0907444994003112.
(56) Pannu, N. S.; Murshudov, G. N.; Dodson, E. J.; Read, R. J. Incorporation of Prior Phase Information Strengthens Maximum-Likelihood Structure Refinement. *Acta Crystallogr. Sect. D Biol. Crystallogr.* **1998**, *54* (6), 1285–1294. https://doi.org/10.1107/S0907444998004119.
(57) Emsley, P.; Lohkamp, B.; Scott, W. G.; Cowtan, K. Features and Development of Coot. *Acta Crystallogr. Sect. D Biol. Crystallogr.* **2010**, *66* (4), 486–501. https://doi.org/10.1107/S0907444910007493.
(58) Krissinel, E.; Henrick, K. Secondary-Structure Matching (SSM), a New Tool for Fast Protein Structure Alignment in Three Dimensions. *Acta Crystallogr. Sect. D Biol. Crystallogr.* **2004**, *60* (12 I), 2256–2268. https://doi.org/10.1107/S0907444904026460.
(59) Pettersen, E. F.; Goddard, T. D.; Huang, C. C.; Couch, G. S.; Greenblatt, D. M.; Meng, E. C.; Ferrin, T. E. UCSF Chimera - A Visualization System for Exploratory Research and Analysis. *J. Comput. Chem.* **2004**, *25* (13), 1605–1612. https://doi.org/10.1002/jcc.20084.
(60) Eggert, C.; Temp, U.; Eriksson, K. E. L. The Ligninolytic System of the White Rot Fungus *Pycnoporus Cinnabarinus*: Purification and Characterization of the Laccase. *Appl. Environ. Microbiol.* **1996**, *62* (4), 1151–1158. https://doi.org/10.1128/aem.62.4.1151-1158.1996.
(61) Krissinel, E.; Henrick, K. Inference of Macromolecular Assemblies from Crystalline State. *J. Mol. Biol.* **2007**, *372* (3), 774–797. https://doi.org/10.1016/j.jmb.2007.05.022.
(62) Boehr, D. D.; Farley, A. R.; Wright, G. D.; Cox, J. R. Analysis of the □ - □ Stacking Interactions between the Aminoglycoside Antibiotic Kinase APH (3 ¯) -IIIa and Its Nucleotide Ligands. **2002**, *9* (02), 1209–1217.
(63) Brylinski, M.; Rouge, B.; Rouge, B. HHS Public Access. **2019**, *91* (2), 380–390.

https://doi.org/10.1111/cbdd.13084.Aromatic.
(64) Hunter, A.; Thornton, J. M. N-N : Interactions : The Geometry and Energetics of Interactions in Proteins ! Y . **1991**.
(65) Lyubimov, A. Y.; Heard, K.; Tang, H.; Sampson, N. S.; Vrielink, A. Distortion of Flavin Geometry Is Linked to Ligand Binding in Cholesterol Oxidase. *Protein Sci.* **2007**, *16* (12), 2647–2656. https://doi.org/10.1110/ps.073168207.
(66) Yoshida, H.; Sakai, G.; Mori, K.; Kojima, K.; Kamitori, S.; Sode, K. Structural Analysis of Fungus-Derived FAD Glucose Dehydrogenase. *Sci. Rep.* **2015**, *5*, 1–13. https://doi.org/10.1038/srep13498.
(67) Lacki, K.; Duvnjak, Z. By Polyphenol Oxidase from the Fungus Trametes Versicolor : Product Elucidation Studies. *Biotechnology* **1998**.
(68) Pardo, I.; Santiago, G.; Gentili, P.; Lucas, F.; Monza, E.; Medrano, F. J.; Galli, C.; Martínez, A. T.; Guallar, V.; Camarero, S. Re-Designing the Substrate Binding Pocket of Laccase for Enhanced Oxidation of Sinapic Acid. *Catal. Sci. Technol.* **2016**, *6* (11), 3900–3910. https://doi.org/10.1039/c5cy01725d.
(69) Camarero, S.; Pardo, I.; Cañas, A. I.; Molina, P.; Record, E.; Martínez, A. T.; Martínez, M. J.; Alcalde, M. Engineering Platforms for Directed Evolution of Laccase from *Pycnoporus Cinnabarinus*. *Appl. Environ. Microbiol.* **2012**, *78* (5), 1370–1384. https://doi.org/10.1128/AEM.07530-11.
(70) Perna, V.; Agger, J. W.; Holck, J.; Meyer, A. S. Multiple Reaction Monitoring for Quantitative Laccase Kinetics by LC-MS. *Sci. Rep.* **2018**, *8* (1). https://doi.org/10.1038/s41598-018-26523-0.
(71) Koschorreck, K.; Richter, S. M.; Ene, A. B.; Roduner, E.; Schmid, R. D.; Urlacher, V. B. Cloning and Characterization of a New Laccase from Bacillus Licheniformis Catalyzing Dimerization of Phenolic Acids. *Appl. Microbiol. Biotechnol.* **2008**, *79* (2), 217–224. https://doi.org/10.1007/s00253-008-1417-2.
(72) Hwang, S.; Lee, C. H.; Ahn, I. S. Product Identification of Guaiacol Oxidation Catalyzed by Manganese Peroxidase. *J.*

Ind. Eng. Chem. **2008**, *14* (4), 487–492. https://doi.org/10.1016/j.jiec.2008.02.008.
(73) Doerge, D. R.; Divi, R. L.; Churchwell, M. I. Identification of the Colored Guaiacol Oxidation Product Produced by Peroxidases. *Anal. Biochem.* **1997**, *250* (1), 10–17. https://doi.org/10.1006/abio.1997.2191.
(74) Aubert, C.; Mathis, P.; Eker, A. P. M.; Brettel, K. Intraprotein Electron Transfer between Tyrosine and Tryptophan in DNA Photolyase from Anacystis Nidulans. *Proc. Natl. Acad. Sci. U. S. A.* **1999**, *96* (10), 5423–5427. https://doi.org/10.1073/pnas.96.10.5423.
(75) Daniel Holu, Hongju M, Norbert Krauß, Tilman Lamparter, Marcus Elstnerac and Natacha Gillet. Functional role of an unusual tyrosine residue in the electron transfer chain of a prokaryotic (6–4) photolyase. *Chemical Science*. **2018**, 1259–1272. https://doi.org/10.1039/c7sc03386a.

List of published manuscripts during the PhD:

- De Sciscio, M. L.; Nardi, A. N.; Parisi, G.; Bulfaro, G.; Costanzo, A.; **Gugole, E**.; Exertier, C.; Freda, I.; Savino, C.; Vallone, B.; Montemiglio, L. C.; D'Abramo, M. Effect of Salts on the Conformational Dynamics of the Cytochrome P450 OleP. *Molecules* **2023**, *28* (2), 1–15. https://doi.org/10.3390/molecules28020832.

-Exertier, C.; Sebastiani, F.; Freda, I.; **Gugole, E**.; Cerutti, G.; Parisi, G.; Montemiglio, L. C.; Becucci, M.; Viappiani, C.; Bruno, S.; Savino, C.; Zamparelli, C.; Anselmi, M.; Abbruzzetti, S.; Smulevich, G.; Vallone, B. Probing the Role of Murine Neuroglobin CDloop-D-Helix Unit in CO Ligand Binding and Structural Dynamics. *ACS Chem. Biol.* **2022 Aug**, *17* (8), 2099–2108. https://doi.org/10.1021/acschembio.2c00172.

-Miceli, M.; Exertier, C.; Cavaglià, M.; **Gugole, E**.; Boccardo, M.; Casaluci, R. R.; Ceccarelli, N.; De Maio, A.; Vallone, B.; Deriu, M. A. ALS2-Related Motor Neuron Diseases: From Symptoms to Molecules. *Biology (Basel).* **2022 Jan**, *11* (1), 10–13. https://doi.org/10.3390/biology11010077.

-Montemiglio, L. C.*; **Gugole, E**.*; Freda, I*.; Exertier, C.; D'auria, L.; Chen, C. G.; Nardi, A. N.; Cerutti, G.; Parisi, G.; D'abramo, M.; Savino, C.; Vallone, B. Point Mutations at a Key Site Alter the Cytochrome P450 OleP Structural Dynamics. *Biomolecules* **2021 Dec**, *12* (1). https://doi.org/10.3390/biom12010055.
*Equally contributing authors

-Exertier, C.; Montemiglio, L. C.; Freda, I.; **Gugole, E**.; Parisi, G.; Savino, C.; Vallone, B. Neuroglobin, Clues to Function and Mechanism. *Mol. Aspects Med.* **2021 Dec**, *84* (September 2021). https://doi.org/10.1016/j.mam.2021.101055.

-Cerutti, G.; **Gugole, E**.*;* Montemiglio, L. C.; Turbé-Doan, A.; Chena, D.; Navarro, D.; Lomascolo, A.; Piumi, F.; Exertier, C.; Freda, I.; Vallone, B.; Record, E.; Savino, C.; Sciara, G. Crystal Structure and

Functional Characterization of an Oligosaccharide Dehydrogenase from Pycnoporus Cinnabarinus Provides Insights into Fungal Breakdown of Lignocellulose. *Biotechnol. Biofuels* **2021 Jul**, *14* (1), 1–18. https://doi.org/10.1186/s13068-021-02003-y.

-Parisi, G.; Freda, I.; Exertier, C.; Cecchetti, C.; **Gugole, E.**; Cerutti, G.; D'auria, L.; Macone, A.; Vallone, B.; Savino, C.; Montemiglio, L. C. Dissecting the Cytochrome P450 Olep Substrate Specificity: Evidence for a Preferential Substrate. *Biomolecules* **2020**, *10* (10), 1–17. https://doi.org/10.3390/biom10101411.